SAE 1050 QUENCHED AND TEMPERED STEEL
ITERATION 61

MONOTONIC AND STRAIN-CONTROLLED TORSION FATIGUE TEST RESULTS

H. Zhang and A. Fatemi

Department of Mechanical, Industrial, and

Manufacturing Engineering

The University of Toledo

Toledo, OH 43606

Prepared for:

American Iron and Steel Institute

February 2003

American Iron and Steel Institute

American Iron and Steel Institute
2000 Town Center, Suite 320
Southfield, Michigan 48075
tel: 248-945-4777
fax: 248-352-1740
www.autosteel.org

NOMENCLATURE

A	cross-sectional area
b, c	axial fatigue strength exponent, fatigue ductility exponent
n, n’	monotonic, cyclic strain hardening exponent
b_0, c_0	shear fatigue strength exponent, fatigue ductility exponent
n_0, n_0’	monotonic, cyclic shear strain hardening exponent
E	modulus of elasticity
G	modulus of rigidity or shear modulus
$G_{midlife}$	modulus of rigidity or shear modulus at midlife
HB, HRC	Brinell, Rockwell C-scale
K, K’	monotonic, cyclic strength coefficient
K_0, K_0’	monotonic, cyclic shear strength coefficient
$N_{50\%}$	number of cycles to midlife
$2N_f$	reversals to failure
$r_{midsection}$	radius to midsection
$r_{surface}$	outer radius
T_f	torque at fracture
T_u	ultimate torque
$\Delta\gamma$	total shear strain range
γ_e, γ_p, γ	elastic, plastic, total shear strain
$\Delta\gamma_p/2$, $\Delta\gamma_p$	plastic shear strain amplitude, range
$\Delta\gamma_e/2$, $\Delta\gamma_e$	elastic shear strain amplitude, range
γ_f, γ_f'	shear fracture strain, shear fracture ductility coefficient
$\gamma_{midsection}$, $\gamma_{surface}$	shear strain at midsection, surface of tube
τ	shear stress
τ_y	shear yeild strength
τ_u	shear ultimate strength
$\Delta\tau/2$, $\Delta\tau$	shear stress amplitude, range
τ_a, τ_m	alternating, mean shear stress
τ_f, τ_f'	shear fracture stress, shear fatigue strength coefficient
$\tau_{midsection}$, $\tau_{surface}$	shear stress at midsection, surface of tube
θ_a	alternating rotational displacement
ε_f'	axial fatigue ductility coefficient
σ_f'	axial fatigue strength coefficient

UNIT CONVERSION TABLE

Measure	SI Unit	US Unit	from SI to US	from US to SI
Length	mm	in	1 mm = 0.03973 in	1 in = 25.4 mm
Area	mm^2	in^2	1 mm^2 = 0.00155 in^2	1 in^2 = 645.16 mm^2
Load	kN	kip	1 kN = 0.2248 kip	1 kip = 4.448 kN
Torque	Nm	lb in	1 Nm = 8.8507 lb in	1 lb in = 0.1130 Nm
Stress	MPa	ksi	1 MPa = 0.14503 ksi	1ksi = 6.895 MPa

In SI Unit:

1 kN = 10^3 N 1 Pa = 1 N/m^2 1 MPa = 10^6 Pa = 1 N/mm^2 1GPa = 10^9 Pa

In US Unit:

1klb = 10^3 lb 1 psi = 1 lb/in^2 1 ksi = 10^3 psi

TABLE OF CONTENTS

SUMMARY

The torsional monotonic properties, and fatigue behavior data have been obtained for SAE 1050 quenched and tempered steel. The material was provided by the American Iron and Steel Institute (AISI). One torsion test was performed to acquire the desired monotonic properties. Twelve strain, rotation or torque-controlled fatigue tests were performed to obtain the strain-life and cyclic stress-strain curves and properties. The experimental procedure followed and results obtained are presented and discussed in this report. Also, comparisons were made to evaluate the current methods of estimating torsional properties from axial properties of this material.

I. EXPERIMENTAL PROGRAM

1.1 Material

The SAE 1050 quenched and tempered steel was manufactured by MacSteel. This material was delivered to the University of Toledo in round bar form. The bars were 1.344 inch in diameter prior to machining. In Table 1, the chemical composition obtained by MacSteel can be seen. The hardness of this material after heat treatment is HRC30. Figure A1 shows the inclusions/voids in longitudinal direction at 100X magnification. Figure A2 shows the microstructure in longitudinal direction at 500X magnification. It can be seen from this photomicrograph that SAE 1050 quenched and tempered steel has a ferrite/pearlite microstructure.

1.2 Specimen

In this study, identical round thin-walled tube specimens were used for the monotonic and fatigue tests. The specimen configuration and dimensions are shown in Figure 1. The specimens were first machined to hollow bars with 3/8" ID, then heat treated to HRC30. After this, they were machined and honed to the final dimensions.

To polish, the specimens were put in a lathe and rotated while three different grits of aluminum oxide lapping film were used. The grits used were 30μ, 15μ, and 3μ. The polishing was then finished using a rotating polishing wheel with a polishing compound resulting in a mirror finish. The rotation of the polishing wheel coincided with the specimen's longitudinal axis. The polished surfaces were carefully examined under magnification to ensure complete removal of machine marks within the test section. The internal and external diameters were measured to the nearest 0.0001 inch. The external

diameter was measured using a micrometer caliper, and the internal diameter was measured using a micrometer and a bore gage.

1.3 Apparatus

An Instron closed-loop servo-controlled hydraulic axial-torsion load frame and digital servo-controller were used to conduct the tests. The calibration of this system was verified prior to beginning the test program. The load cell used had a capacity of 8850 lb-in in torsion and 22,480 lb axially. Hydraulically operated grips using universal tapered collets were employed to secure the specimens' ends in series with the load cell.

Total shear strain was controlled for all tests using an Epsilon axial-torsion extensometer. The calibration of the extensometer was verified using a specimen fitted with strain gages and the calibration apparatus provided by the manufacturer. The extensometer had a gage length of 1 inch and had a shear strain angle range of ±2.5° (±5° angle of twist on 1.0 in. diameter Specimen). In order to protect the specimens' surface from the contact points of the extensometer, ASTM Standard E606 [1] recommends the use of transparent tape or epoxy to 'cushion' the attachment. For this study, it was found that application of three layers of transparent tape effectively cushioned the extensometer when the extensometer springs had been adjusted properly.

The load train (load cell, grips, specimen, and actuator) was checked for proper alignment. Misalignment can result from both tilt and offset between the central lines of the load train components. According to ASTM Standard E606 [1], the maximum bending strains should not exceed 5 % of the minimum axial strain range imposed during any test program. To test this, two arrays of four strain gages per array were arranged at the upper

and lower ends of the uniform gage section. For each array, gages were equally spaced around the circumference of a 0.61-in. diameter specimen with uniform gage section. The maximum bending strain determined from the specimen fitted with strain gages was less than 20 microstrain. This value was well within the allowable ASTM limit.

1.4 Test Methods and Procedures

1.4.1 Monotonic torsion tests

One specimen was used to obtain the monotonic properties. Due to the limitations of the extensometer, strain control was used only up to a shear strain of 0.035. After this point, the extensometer was removed and rotational displacement control was used until fracture. For the entire strain-controlled portion (0 to 0.035 shear strain), a strain rate of 0.0002 shear strain/sec was chosen. After this a rotation rate of 0.07 degrees/sec. was chosen to give a similar strain rate. For these tests the axial channel was run in load control allowing the specimen to change in length and avoiding axial stress.

1.4.2 Constant amplitude torsion fatigue tests

There are no ASTM standards for torsion fatigue testing. ASTM Standard E606 [1] for axial strain-controlled fatigue testing recommends at least 10 specimens be used to generate the axial fatigue properties of a material. For this torsion study, 12 specimens at 7 different shear strain amplitudes ranging from 0.00425 to 0.03 were utilized resulting in lives between several hundred and more than one million cycles. The Instron software Max was used to record the hysteresis loops at intervals of 2^n.

There were two control modes used for these tests. All tests were run in strain control until the estimated midlife and then changed over to rotation control. The reason for the change in control mode was for the protection of the extensometer. For the strain-controlled tests, the applied frequencies ranged from 0.10 Hz to 0.50 Hz. For the rotation controlled tests, the frequencies ranged from 0.1 to 3 Hz. For some tests, after switching to rotation control the frequency was increased in order to shorten the overall test duration. All tests were conducted at room temperature and using a sinusoidal waveform.

II. EXPERIMENTAL RESULTS AND ANALYSIS

2.1 Monotonic Deformation Behavior

The properties determined from monotonic tests were the following: modulus of rigidity or shear modulus (G), shear yield strength (τ_y), ultimate shear strength (τ_u), shear fracture strength (τ_f), shear strength coefficient (K_0), and shear strain hardening exponent (n_0).

Shear stress (τ), strain (γ), and plastic strain (γ_p) for the specimen midsection were calculated from the measured torque and the specimen dimensions:

$$\tau_{\text{midsection}} = \frac{T}{A\, r_{\text{midsection}}} \tag{1a}$$

$$\gamma_{\text{midsection}} = \gamma_{\text{surface}} \left(\frac{r_{\text{midsection}}}{r_{\text{surface}}} \right) \tag{1b}$$

$$\gamma_{\text{p\_midsection}} = \gamma_{\text{midsection}} - \frac{\tau_{\text{midsection}}}{G} \tag{1c}$$

Note that the difference between $\tau_{\text{midsection}}$ calculated from Equation (1a) and from $\tau = Tr/J$ for a thin-walled tube with outside and inside diameters of 0.6 in and 0.5 in, respectively, is less than 1%. Either equation can be used for elastic as well as inelastic behavior. Equation (1b) is used to extrapolate the surface shear strain controlled in the test to the midsection shear strain. This linear extrapolation applies to both elastic as well as inelastic deformations.

The modulus of rigidity or shear modulus (G) was determined by calculating the slope of the elastic region of the monotonic curves. Therefore,

$$G = \frac{\Delta \tau_{\text{surface}}}{\Delta \gamma_{\text{surface}}} \tag{2}$$

The shear yield strength (τ_y) was determined by using the 0.2% offset method on the monotonic shear stress-strain curve. The ultimate shear strength (τ_u) and shear fracture strength were calculated using:

$$\tau_u = \frac{T_u}{A\, r_{midsection}} \tag{3}$$

and

$$\tau_f = \frac{T_f}{A\, r_{midsection}} \tag{4}$$

respectively, where T_u is the ultimate or maximum torque and T_f is the torque at fracture. Shear fracture strain (γ_f) was not attained because the extensometer was removed before fracture.

Analogous to axial stress-strain representation, the shear stress (τ) - shear strain (γ) relation is also often represented by the Ramberg-Osgood equation:

$$\gamma = \gamma_e + \gamma_p = \frac{\tau}{G} + \left(\frac{\tau}{K_0}\right)^{\frac{1}{n_0}} \tag{5}$$

The shear strength coefficient, K_0, and strain hardening exponent, n_0, are the intercept and slope of the best line fit to shear stress (τ) versus plastic shear strain (γ_p) data in log-log scale:

$$\tau = K_0\left(\gamma_p\right)^{n_0} \tag{6}$$

The shear stress and plastic shear strain used were for the specimen midsection. When performing the least squares fit, the plastic shear strain (γ_p) was the independent variable and the stress (τ) was the dependent variable in accordance with ASTM Standard E739 [2]. Figure 2 shows the torque versus rotation curve from monotonic test. The monotonic shear

stress-strain curve is shown in Figure 3. The plot used to determine K_0 and n_0 can be seen in Figure 4. The valid data range used was between the end of the yield point strain and the shear strain at which the extensometer was removed. A summary of the results from monotonic torsion test is shown in Table A.1 and these values are also listed in Table 4.

2.2 Cyclic Deformation Behavior

2.2.1 Transient cyclic response

Transient cyclic response describes the process of cyclic-induced change in deformation resistance of a material. Data obtained from constant amplitude fatigue tests were used to determine this response. Plots of stress amplitude variation versus applied number of cycles in strain-controlled or rotation-controlled tests can indicate the degree of transient cyclic softening/hardening. Also, these plots show when cyclic stabilization occurs. A composite plot of the transient normalized cyclic response for SAE 1050 quenched and tempered steel is shown in the rectangular plot in Figure A3, while a semi-log plot is shown in Figure A4. These figures indicate cyclic stability is achieved early during the cyclic deformation process. Even though multiple tests were conducted at some strain amplitude levels, results from one test at each level are shown in these figures.

2.2.2 Steady-state cyclic deformation

Another cyclic behavior of interest was the steady state or stable response. Data obtained from constant amplitude fatigue tests were also used to determine this response. The properties determined from the steady-state hysteresis loops were the following: cyclic shear strength coefficient (K_0'), and cyclic shear strain hardening exponent (n_0'). Half-life

(midlife) hysteresis loops and data were used to obtain the stable cyclic shear properties. Similar to monotonic behavior, the cyclic shear stress-strain behavior can be characterized by the Ramberg-Osgood type equation:

$$\gamma_a = \gamma_e + \gamma_p = \frac{\tau_a}{G} + \left(\frac{\tau_a}{K_0'} \right)^{\frac{1}{n_0'}} \tag{7}$$

It should be noted that in Equation (7) and the other equations that follow, G is the shear modulus that was measured from the monotonic test. The cyclic shear strength coefficient, K_0', and cyclic shear strain hardening exponent, n_0', are the intercept and slope of the best line fit to shear stress amplitude ($\Delta\tau/2$) versus plastic shear strain amplitude ($\Delta\gamma_p/2$) data in log-log scale:

$$\frac{\Delta\tau}{2} = K_0' \left(\frac{\gamma_p}{2} \right)^{n_0'} \tag{8}$$

When performing the least squares fit, the plastic shear strain amplitude ($\Delta\gamma_p/2$) was the independent variable and the shear stress amplitude ($\Delta\tau/2$) was the dependent variable as is done for axial testing in accordance with ASTM Standard E739 [2]. Shear stress amplitudes were calculated from Equation (1a) for specimen midsection at or near midlife. Plastic shear strain amplitudes for midsection were calculated by the following equation:

$$\left(\frac{\Delta\gamma_p}{2} \right)_{\text{midsection}} = (\gamma_a)_{\text{midsection}} - \frac{(\tau_a)_{\text{midsection}}}{G_{\text{midlife}}} \tag{9}$$

This plot is shown in Figure 5. To generate the K_0' and n_0' values, all data were used. The curve showing the Ramberg-Osgood equation and the data can be seen in Figure 6.

The cyclic stress-strain curve reflects the resistance of a material to cyclic deformation and can be vastly different from the monotonic stress - strain curve. In Figure

7, superimposed plots of monotonic and cyclic curves are shown. As can be seen in Figure 7, SAE 1050 quenched and tempered steel cyclically softens. Figure A5 shows a composite plot of the steady-state (midlife) hysteresis loops. Even though multiple tests were conducted at some levels, the loop from only one test is shown from each shear strain level. Tables 2 and 3 provide the summary of the fatigue test results and fatigue test calculations, respectively.

2.3 Constant Amplitude Torsional Fatigue Behavior

Constant amplitude strain-controlled torsion fatigue tests were performed to determine the shear strain-life curve. Analogous to the Coffin-Manson equation for axial fatigue behavior, the following equation relates the shear strain amplitude to the fatigue life:

$$\frac{\Delta\gamma}{2} = \frac{\Delta\gamma_e}{2} + \frac{\Delta\gamma_p}{2} = \frac{\tau_f'}{G}(2N_f)^{b_0} + \gamma_f'(2N_f)^{c_0} \qquad (10)$$

where τ_f' is the shear fatigue strength coefficient, b_0 is the shear fatigue strength exponent, γ_f' is the shear fatigue ductility coefficient, c_0 is the shear fatigue ductility exponent, G is the shear modulus, and $2N_f$ is the number of reversals to failure (which was defined as a 10% torsional load drop).

The shear fatigue strength coefficient, τ_f', and shear fatigue strength exponent, b_0, are the intercept and slope of the best line fit to shear stress amplitude ($\Delta\tau/2$) versus reversals to failure ($2N_f$) data in log-log scale:

$$\frac{\Delta\tau}{2} = \tau_f'(2N_f)^{b_0} \qquad (11)$$

When performing the least squares fit, the shear stress amplitude ($\Delta\tau/2$) was the independent variable and the reversals to failure ($2N_f$) was the dependent variable as is done for axial

testing in accordance with ASTM Standard E739 [2]. This plot is shown in Figure 8. To generate the τ_f' and b_0 values, the range of data used in this figure was chosen for $N_f < 10^6$ cycles. The shear fatigue ductility coefficient, γ_f', and shear fatigue ductility exponent, c_0, are the intercept and slope of the best line fit to calculated shear plastic strain amplitude ($\Delta\gamma_p/2$) versus reversals to failure ($2N_f$) data in log-log scale:

$$\left(\frac{\Delta\gamma_p}{2}\right)_{calculated} = \gamma_f'\left(2N_f\right)^{c_0} \tag{12}$$

When performing the least squares fit, the calculated shear plastic strain amplitude ($\Delta\gamma_p/2$) was the independent variable and the reversals to failure ($2N_f$) was the dependent variable as is done in axial testing in accordance with ASTM Standard E739 [2]. The calculated shear plastic strain amplitude was determined from Equation 12. This plot is shown in Figure 9. Figure 10 shows the same plot with measured plastic shear strain amplitude values. As can be seen, similar results are obtained. To be consistent with the procedure used for axial strain-controlled fatigue property determinations by AISI, the plot with the calculated plastic shear strain amplitudes was used to obtain γ_f' and c_0. The data range used in these plots was chosen for $N_f < 10^6$ cycles.

The total shear strain amplitude versus reversals to failure plot is shown in Figure 11. This plot displays the shear strain-life curve (Eqn.10), the elastic shear strain portion (Eqn. 11), the plastic shear strain portion (Eqn.12), and superimposed torsion fatigue data. A summary of the cyclic properties for SAE 1050 quenched and tempered steel is provided in Table 4.

III. PREDICTIONS AND FAILURE MECHANISMS

3.1 Predictions from axial data

Common failure criteria were used to predict the torsional behavior of the material from axial data. The axial tests data used are from SAE 1045 steel (BHN 277). This is because the axial fatigue properties of 1050 steel at HRC30 (BHN 285) was not available. The axial monotonic and cyclic properties of this material were obtained by the SAE Fatigue Design and Evaluation Committee [3]. Experimentally obtained monotonic and cyclic data for both axial and torsional tests of both materials are summarized in Table 5. The torsional monotonic curve was compared to the von Mises and the Tresca predictions. This was done by using the Ramberg-Osgood equation:

$$\gamma = \gamma_e + \gamma_p = \frac{\tau}{G} + \left(\frac{\tau}{K_0}\right)^{\frac{1}{n_0}} \tag{13}$$

where K_0 and n_0 are computed using predictions based on von Mises criterion [4]:

$$K_0 = K(1/3)^{(n+1)/2} \quad \text{and} \quad n_0 = n \tag{14}$$

resulting in $K_0 = 494$ MPa and $n_0 = 0.0548$, and predictions based on Tresca criterion:

$$K_0 = \frac{K}{2}(2/3)^n \quad \text{and} \quad n_0 = n \tag{15}$$

resulting in $K_0 = 431$ MPa and $n_0 = 0.0548$. Note that from the torsion test, $K_0 = 781$MPa and $n_0 = 0.1574$. This comparison can be seen in Figure 12. It can be seen from this figure that the von Mises estimation fits the actual data better than the Tresca prediction.

The next prediction is for the cyclic deformation curve. This was done using the same equations as with the monotonic curves (Equations 14 and 15), except with n_0' and K_0' being calculated using n' and K' from the axial cyclic properties. The von Mises criterion

results in K_0' = 907 MPa, and n_0' = 0.1887, while the Tresca criterion results in K_0' = 808 MPa, and n_0' = 0.1887. Note that from the torsion test data K_0' = 699 MPa, and n_0' = 0.1391. These constants were then used in the following equation to represent the shear stress-shear strain relationship:

$$\gamma_a = \gamma_e + \gamma_p = \frac{\tau_a}{G} + \left(\frac{\tau_a}{K_0'} \right)^{\frac{1}{n_0'}} \tag{16}$$

This comparison can be seen in Figure 13. This figure shows that in lower strain range (up to 2% shear strain), the von Mises criterion provides better estimations while in higher strain range, the Tresca criterion provides better estimations.

The final predictions made were for the fatigue data. The torsional strain-life equation:

$$\frac{\Delta\gamma}{2} = \frac{\Delta\gamma_e}{2} + \frac{\Delta\gamma_p}{2} = \frac{\tau_f'}{G}(2N_f)^{b_0} + \gamma_f'(2N_f)^{c_0} \tag{17}$$

was used, where τ_f' and γ_f' were calculated for the von Mises criterion using:

$$\tau_f' = \sigma'_f / \sqrt{3}, \qquad \gamma_f' = \sqrt{3}\varepsilon_f', \quad b_0 = b, \text{ and } \quad c_0 = c \tag{18}$$

resulting in τ_f' = 1720 MPa, γ_f' = 1.212, b_0 = -0.158, and c_0 = -0.578. For the Tresca criterion:

$$\tau_f' = \sigma'_f / 2, \qquad \gamma_f' = 1.5\varepsilon_f', \quad b_0 = b, \text{ and } \quad c_0 = c \tag{19}$$

were used resulting in τ_f' = 1489 MPa, γ_f' = 1.05, b_0 = -0.158, and c_0 = -0.578. Note that from torsion tests τ_f' = 652 MPa, γ_f'= 0.4182, b_0 = -0.0684, and c_0 = -0.4492. This comparison can be seen in Figure 14. This figure shows that overall, the von Mises criterion provides better estimations, except in the low cycle region ($<10^3$ cycles) where the Tresca criterion provides better estimations.

3.2 Predictions from Hardness

A simple method for the estimation of axial fatigue properties from Brinell hardness and elastic modulus of steels has been proposed by Roessle and Fatemi [5]. This method is valid for hardness between 150 and 700HB and uses the following etimates:

$$\sigma_f' = 4.25(HB) + 225 \tag{20}$$

$$\varepsilon_f' = \frac{1}{E}\left[0.32(HB)^2 - 487(HB) + 191000\right] \tag{21}$$

$b_0 = -0.09$, and $c_0 = -0.56$ (22)

A comparison of the predicted axial fatigue curve with the experimental axial curve is shown in Figure 15. In this figure, two materials with different hardness were used for the comparison. One is SAE 1050 steel at BHN205, the other is SAE 1045 steel at BHN277. Figure 15 shows that this method provides better estimations for SAE 1050 steel (BHN205). It may be concluded that this estimation for 1050 steel at BHN205 based on hardness will also apply to the 1050 steel at BHN285.

Combining Equations (20) through (22) with Equations (17) through (19) gives three new estimations of torsional fatigue properties based on hardness. The substitution for von Mises criterion results in:

$$\frac{\Delta\gamma}{2} = \frac{[4.25(HB) + 225]}{\sqrt{3}G}\left(2N_f\right)^{-0.09} + \frac{\sqrt{3}}{E}[0.32(HB)^2 - 487(HB) + 191000]\left(2N_f\right)^{-0.56} \tag{23}$$

for Tresca criterion:

$$\frac{\Delta\gamma}{2} = \frac{[4.25(HB) + 225]}{2G}\left(2N_f\right)^{-0.09} + \frac{1.5}{E}[0.32(HB)^2 - 487(HB) + 191000]\left(2N_f\right)^{-0.56} \tag{24}$$

Using SAE 1050 steel (BHN 285), the results of Equations (23) and (24) were compared with the tortional experiment strain-life curve in Figure 16. It shows that the von Mises criterion provides better estimations than the Tresca criterion.

3.3 Failure Mode

Cracks on the specimens were observed to be in one of the maximum shear planes, all parallel to the axis of the specimen. In Figure 17, a typical specimen is shown with a longitudinal fatigue crack.

REFERENCES

[1] ASTM Standard E606-92, "Standard Practice for Strain-Controlled Fatigue Testing," Annual Book of ASTM Standards, Vol. 03.01, 1997, pp. 198-206.

[2] ASTM Standard E739-91, "Standard Practice for Statistical Analysis of Linear or Linearized Stress-Life (S-N) and Strain-Life (ε-N) Fatigue Data," Annual Book of ASTM Standards, Vol. 03.01, 1995, pp. 615-621.

[3] Dindinger, P., Kurath, P., Langner, M., "Summary of the Experimental Program: Induction Hardened Notched Shaft", *Multiaxial Fatigue of an Induction Hardened Shaft, AE-28*, Society of Automotive Engineers, Inc. Warrendale, Pa., pp. 3-22.

[4] Dowling, N. E., "Mechanical Behavior of Materials: Engineering Methods for Deformation, Fracture, and Fatigue," 2nd Edition, Prentice-Hall, Inc., 1999.

[5] Roessle M. L., Fatemi, A., "Strain-controlled fatigue properties of steels and some simple approximations," *International Journal of Fatigue*, Vol. 22, 2000, pp. 495-511.

Table 1: Chemical composition of SAE 1050 Quenched and Tempered steel

Carbon, C	0.50%
Manganese, Mn	0.70%
Phosphorous, P	0.013%
Sulfur, S	0.029%
Silicon, Si	0.23%
Copper, Cu	0.12%
Nickel, Ni	0.07%
Chromium, Cr	0.17%
Molybdenum, Mo	0.03%
Aluminum, Al	0.025%
Calcium, Ca	0.0009%
Tin, Sn	0.006%

Table 2: Torsion fatigue test results

Specimen ID	OD, mm (in.)	ID, mm (in)	$G_{initial}$, MPa (ksi)	Testing control mode	Test frequency, Hz	Mid-life measurements					$N_{50\%}$, cycles	N_f, cycles
						$\gamma_{a\ surface}$	$\gamma_{m\ surface}$	T_a, Nm (lb.in)	T_m, Nm (lb.in)	θ_a degrees		
T1	15.47 0.6092	12.75 0.5019	81624 (11838)	Strain Rotation	0.10 0.10	3.011%	0.000%	180.8 (1600.2)	0.08 (0.7)	9.00	158	377
T14	15.43 0.6073	12.71 0.5003	79037 (11463)	Strain Rotation	0.10 0.10	3.002%	0.000%	176.0 (1558.2)	0.01 (0.1)	8.70	177	438
T3	15.45 0.6082	12.70 0.5000	78683 (11411)	Strain	0.20	1.999%	0.000%	162.0 (1434.1)	-0.03 -(0.2)	5.99	256	668
T12	15.39 0.6061	12.75 0.5018	77339 (11216)	Strain Rotation	0.20 0.20	2.000%	-0.001%	157.7 (1396.1)	-0.03 -(0.2)	5.83	612	1,042
T20	15.45 0.6082	12.70 0.5001	78153 (11334)	Strain Rotation	0.30 0.30	1.349%	0.000%	148.8 (1316.8)	-0.02 -(0.2)	4.13	712	1,581
T10	15.47 0.6090	12.90 0.5078	73748 (10695)	Strain	0.50	0.998%	-0.001%	125.8 (1113.3)	-0.17 -(1.5)	3.17	4,096	7,396
T17	15.47 0.6091	12.91 0.5083	82384 (11948)	Strain Rotation	0.50 0.50	1.000%	0.000%	130.1 (1151.8)	-0.02 -(0.2)	3.27	2,448	4,349
T18	15.44 0.6079	12.94 0.5093	77983 (11310)	Strain Rotation	0.50 0.80	0.750%	-0.001%	121.2 (1072.8)	-0.18 -(1.6)	2.42	16,784	34,976
T2	15.45 0.6081	12.90 0.5078	80342 (11652)	Strain Rotation	0.50 1	0.594%	0.002%	118.3 (1047.2)	-0.48 -(4.3)	2.06	33,213	84,718
T19	15.45 0.6084	13.06 0.5141	76923 (11156)	Strain Rotation	0.50 1	0.600%	0.000%	112.6 (996.2)	0.11 (0.9)	1.98	65,990	99,138
T7	15.43 0.6076	12.80 0.5039	77659 (11263)	Strain Rotation	0.50 3	0.425%	0.000%	100.3 (887.4)	-0.39 -(3.4)	1.48	524,738	>1,000,000
T15	15.45 0.6084	12.91 0.5084	77184 (11194)	Strain Rotation	0.50 3	0.422%	-0.002%	103.1 (912.1)	-0.23 -(2.0)	1.55	526,288	>1,000,000

Table 3: Torsion fatigue test calculation results

Specimen ID	$G_{first\ cycle}$, MPa (ksi)	$G_{midlife}$, MPa (ksi)	Midlife Values											$2N_{50\%}$, cycles	$2N_f$, cycles
			Surface						Midsection						
			γ_a	γ_m	$(\Delta\gamma_p/2)_{meas}$, %	$(\Delta\gamma_p/2)_{calc}$ %	τ_a, MPa (ksi)	τ_m, MPa (ksi)	γ_a	γ_m	$(\Delta\gamma_p/2)_{calc}$ %	τ_a, MPa (ksi)	τ_m, MPa (ksi)		
T1	81624	72687	3.011%	0.000%	2.311%	2.419%	430.5	0.2	2.746%	0.000%	2.162%	424.2	0.2	316	754
	(11838.2)	(10542.0)					62.4	0.0				(61.5)	(0.0)		
T14	79037	69483	3.002%	0.000%	2.281%	2.393%	423.0	0.0	2.737%	0.000%	2.137%	416.8	0.0	354	876
	(11463.0)	(10077.3)					61.4	0.0				(60.5)	(0.0)		
T3	78683	70574	1.999%	0.000%	1.373%	1.453%	385.4	-0.1	1.821%	0.000%	1.284%	379.0	-0.1	512	1,336
	(11411.7)	(10235.5)					55.9	0.0				(55.0)	(0.0)		
T12	77339	69035	2.000%	-0.001%	1.367%	1.436%	389.5	-0.1	1.828%	-0.001%	1.273%	382.9	-0.1	1,224	2,084
	(11216.7)	(10012.4)					56.5	0.0				(55.5)	(0.0)		
T20	78153	73286	1.349%	0.000%	0.772%	0.865%	354.9	0.0	1.230%	0.000%	0.754%	348.2	0.0	1,424	3,162
	(11334.8)	(10628.8)					51.5	0.0				(50.5)	(0.0)		
T10	73749	69326	0.998%	-0.001%	0.488%	0.542%	316.6	-0.4	0.915%	-0.001%	0.469%	309.7	-0.4	8,192	14,792
	(10696.0)	(10054.6)					45.9	-0.1				(44.9)	-(0.1)		
T17	82384	71458	1.000%	0.000%	0.500%	0.537%	331.3	-0.1	0.917%	0.000%	0.468%	321.4	-0.1	4,896	8,698
	(11948.4)	(10363.8)					48.1	0.0				(46.6)	(0.0)		
T18	77983	70869	0.750%	-0.001%	0.295%	0.308%	313.3	-0.5	0.690%	-0.001%	0.258%	306.1	-0.5	33,568	69,952
	(11310.1)	(10278.4)					45.4	-0.1				(44.4)	-(0.1)		
T2	80343	79766	0.594%	0.002%	0.195%	0.217%	300.9	-1.2	0.545%	0.002%	0.176%	294.4	-1.2	66,426	169,436
	(11652.3)	(11568.7)					43.6	-0.2				(42.7)	-(0.2)		
T19	76924	73288	0.600%	0.000%	0.180%	0.189%	300.9	0.3	0.553%	0.000%	0.152%	294.4	0.3	131,980	198,276
	(11156.4)	(10629.1)					43.6	0.0				(42.7)	(0.0)		
T7	77659	72903	0.425%	0.000%	0.072%	0.076%	254.9	-1.0	0.389%	0.000%	0.055%	243.2	-0.9	1,049,476	>2,000,000
	(11263.1)	(10573.3)					37.0	-0.1				(35.3)	-(0.1)		
T15	77184	80000	0.422%	-0.002%	0.075%	0.085%	269.1	-0.6	0.387%	-0.002%	0.066%	256.8	-0.6	1,052,576	>2,000,000
	(11194.2)	(11602.6)					39.0	-0.1				(37.2)	-(0.1)		

Table 4: Summary of torsion properties

Monotonic Properties			
Hardness , Rockwell C (HRC)		30	
Hardness , Brinell (BHN)		285	
Modulus of Rigidity, G, GPa (ksi):		77.8	(11278)
Shear Yield Strength, τ_y, MPa (ksi):		366.5	(53.2)
Shear ultimate strength, τ_u, MPa (ksi):		585.7	(85.0)
Shear fracture strain, γ_f:		N/A	-
Shear fracture stress, τ_f, Mpa (ksi):		335.6	(48.7)
Shear strength coefficient, K_0, MPa (ksi):		780.8	(113.2)
Shear strain hardening exponent, n_0:		0.1574	-
Cyclic Properties			
Cyclic shear yield strength, τ_y' (0.2% offset) = $K_0'(0.002)^{n0'}$, MPa (ksi)		294.5	(42.7)
Cyclic shear strength coefficient, K_0', MPa (ksi):		699.0	(101.4)
Cyclic shear strain hardening exponent, n_0':		0.1391	-
Fatigue shear strength coefficient, τ_f', MPa (ksi):		652.3	(94.6)
Fatigue shear strength exponent, b_0:		-0.0684	-
Fatigue shear ductility coefficient, γ_f':		0.4182	-

Table 5: Comparison of axial (SAE 1045 steel BHN 277) and torsional (SAE 1050 steel BHN 285) properties

Monotonic Properties	Axial (1045 steel BHN 277)			Torsional (1050 steel BHN 285)		
Modulus, GPa (ksi):	E =	206.0	(29877)	G =	77.8	(11278)
Yield strength, MPa (ksi):	σ_y =	619.0	(89.8)	τ_y =	366.5	(53.2)
Ultimate strength, MPa (ksi):	σ_u =	942.0	(136.6)	τ_u =	585.7	(85)
Fracture stress, MPa (ksi)	σ_f =	-	-	τ_f =	335.6	(48.7)
Strength coefficient, MPa (ksi):	K =	882	(127.9)	K_o =	781	(113.2)
Strain hardening exponent:	n =	0.0548		n_o =	0.1574	
Cyclic Properties						
Cyclic yield strength, MPa (ksi)	σ_y' =	539.6	(78.3)	τ_y' =	294.5	(42.7)
Cyclic strength coefficient, MPa (ksi):	K' =	1,743.4	(252.8)	K_o' =	699.0	(101.4)
Cyclic strain hardening exponent:	n' =	0.1887		n_o' =	0.1391	
Fatigue strength coefficient, MPa (ksi):	σ_f' =	2,978.4	(432.0)	τ_f' =	652.3	(94.6)
Fatigue strength exponent:	b =	-0.158		b_o =	-0.0684	
Fatigue ductility coefficient:	ε_f' =	0.700		γ_f' =	0.4182	
Fatigue ductility exponen:	c =	-0.578		c_o=	-0.4492	

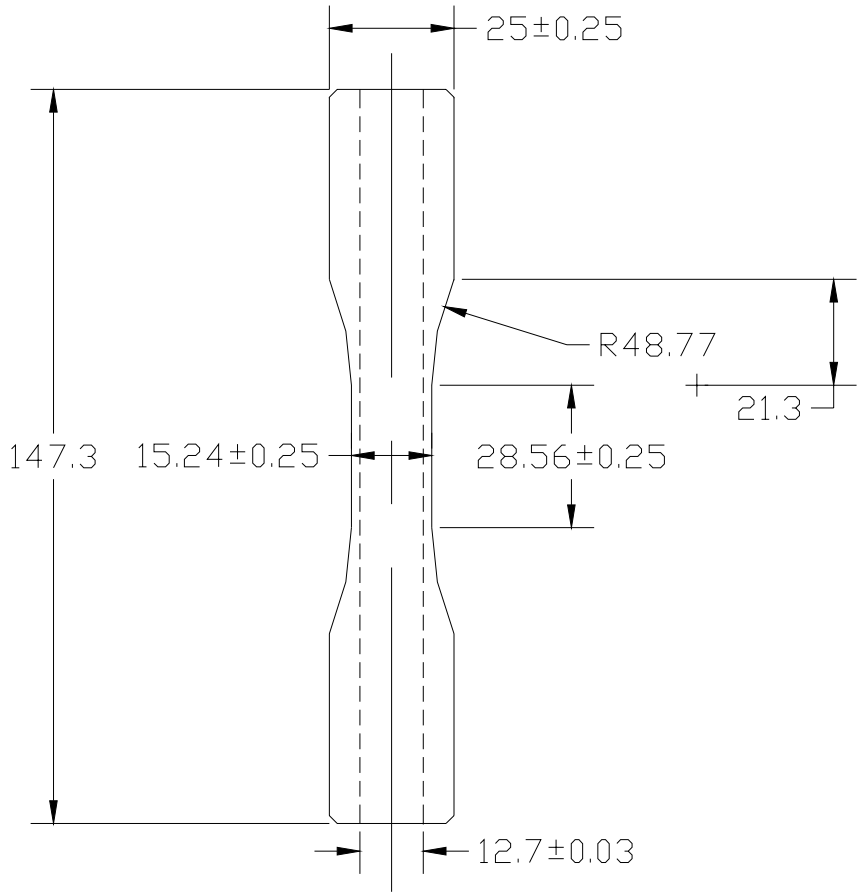

Figure 1: Specimen configuration and dimensions (all dimensions in milimeters)

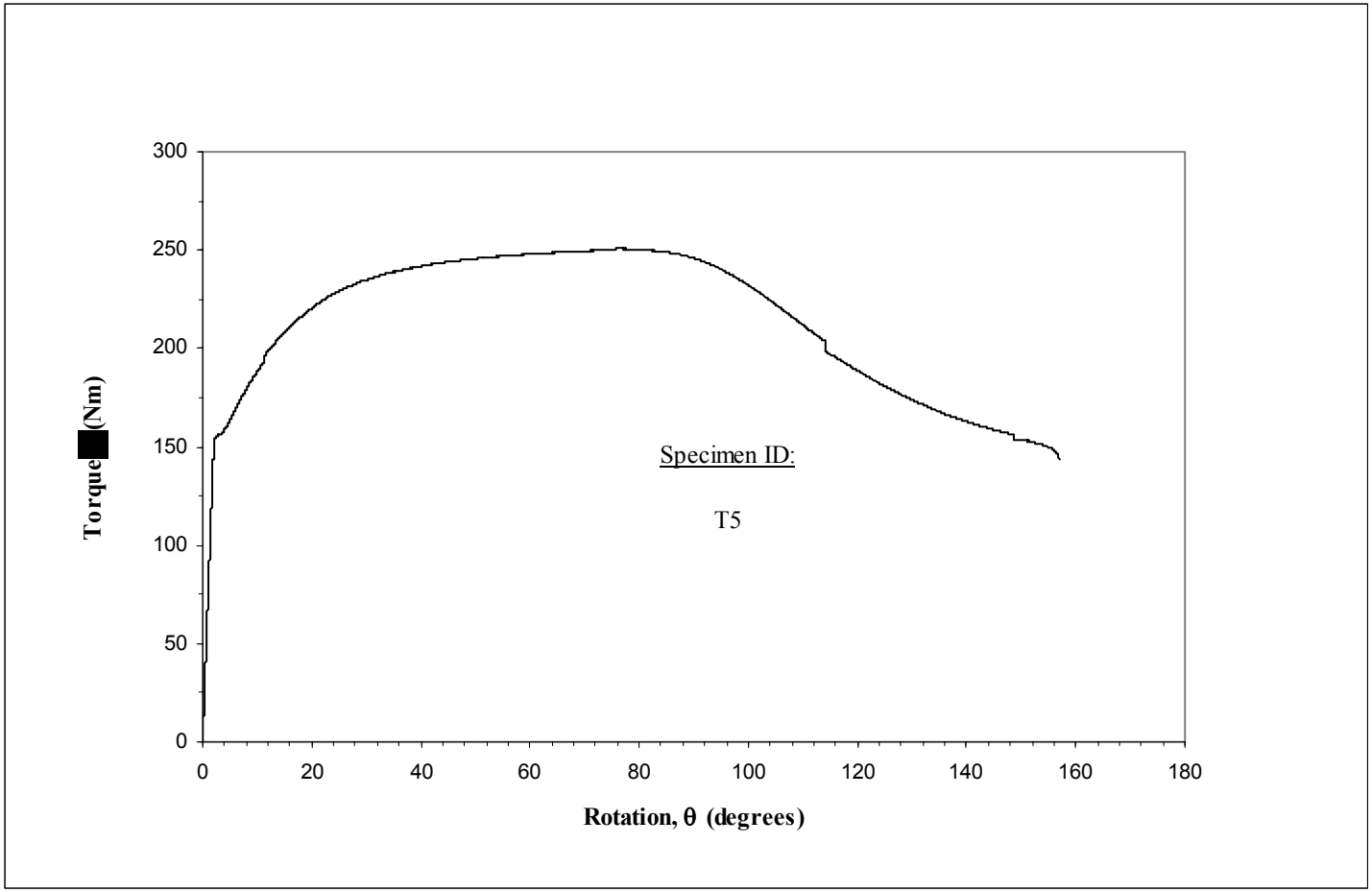

Figure 2: Monotonic torque versus rotation curve

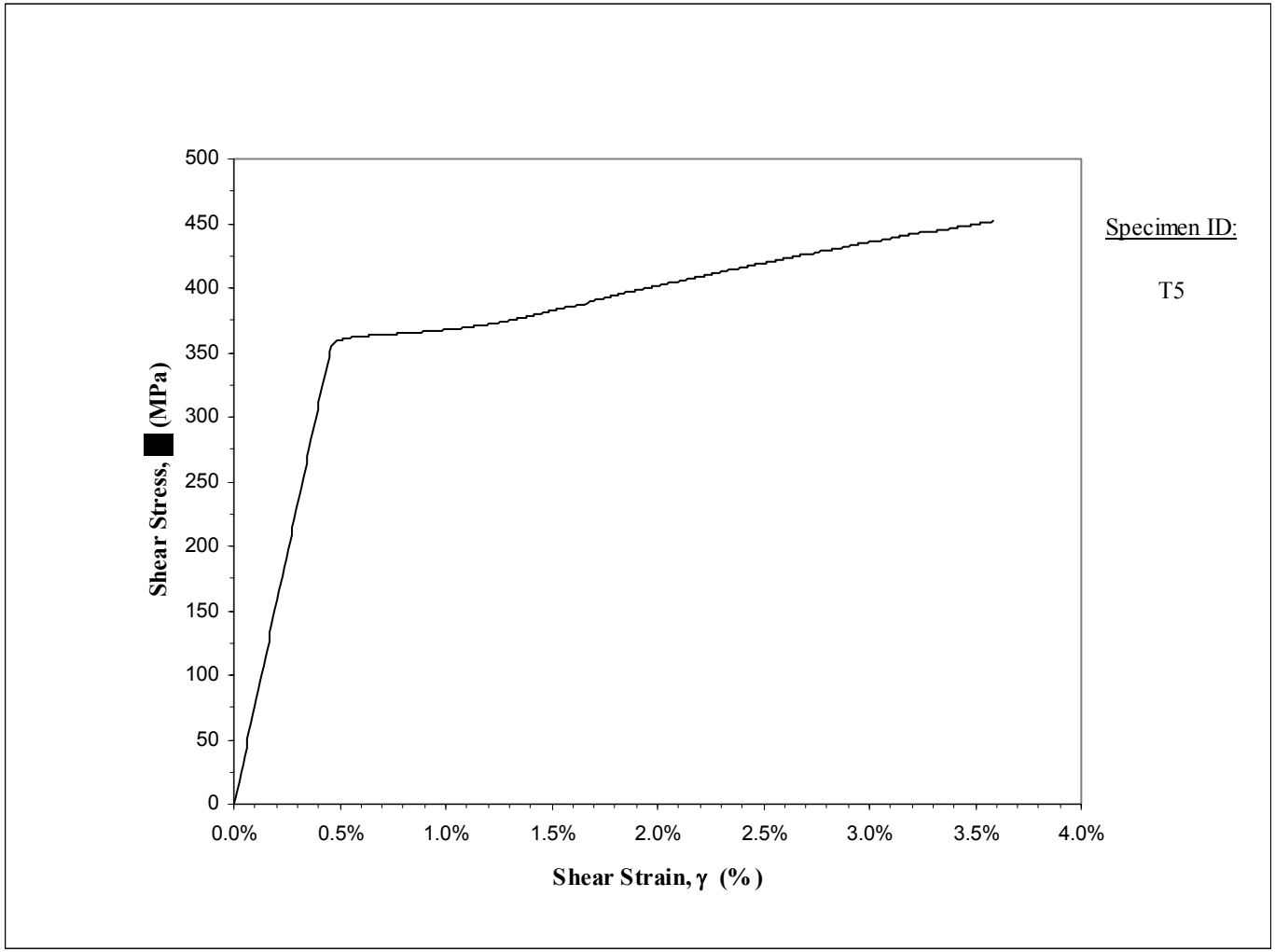

Figure 3: Monotonic shear stress-strain curve

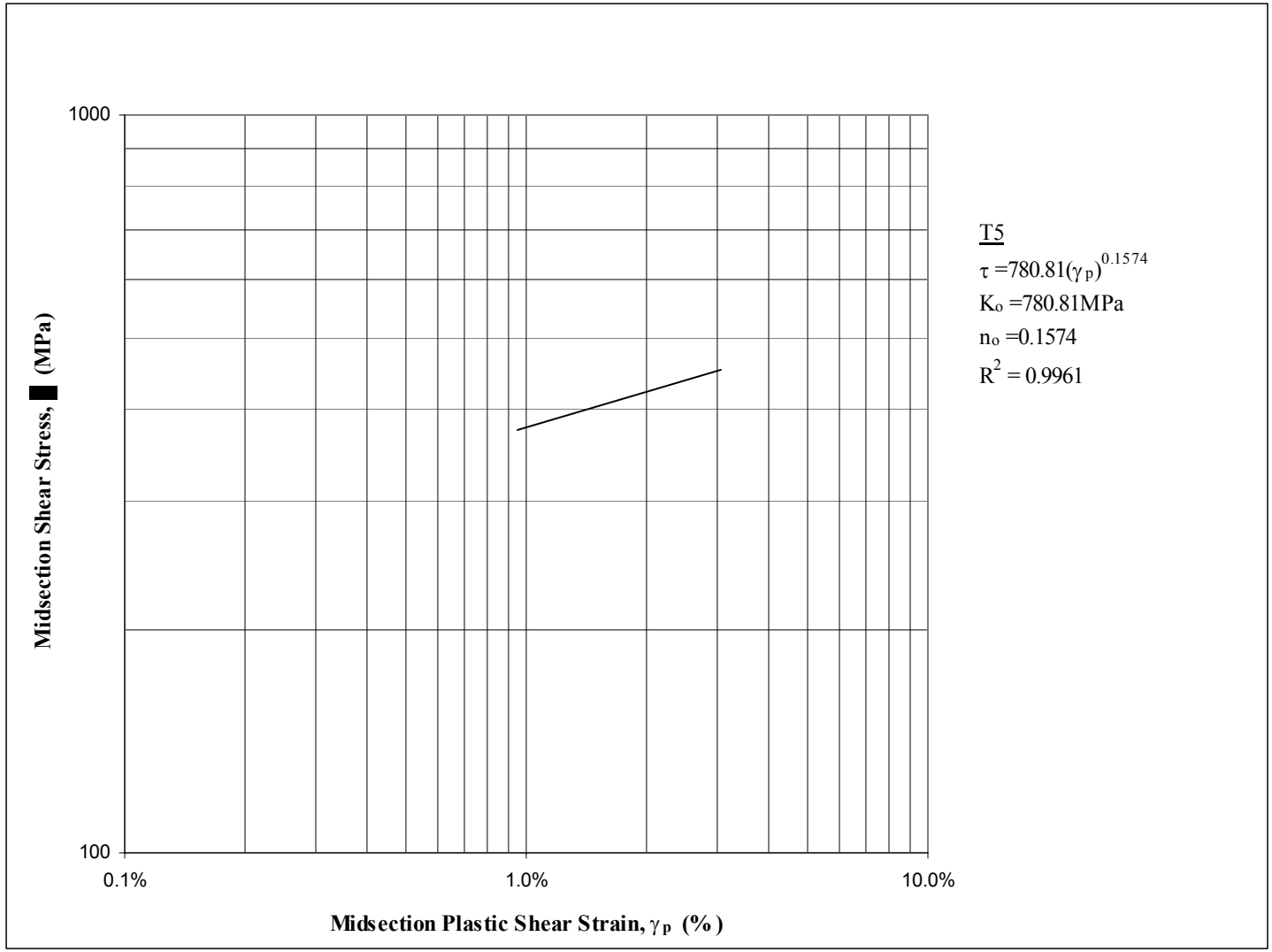

Figure 4: Shear stress versus plastic shear strain

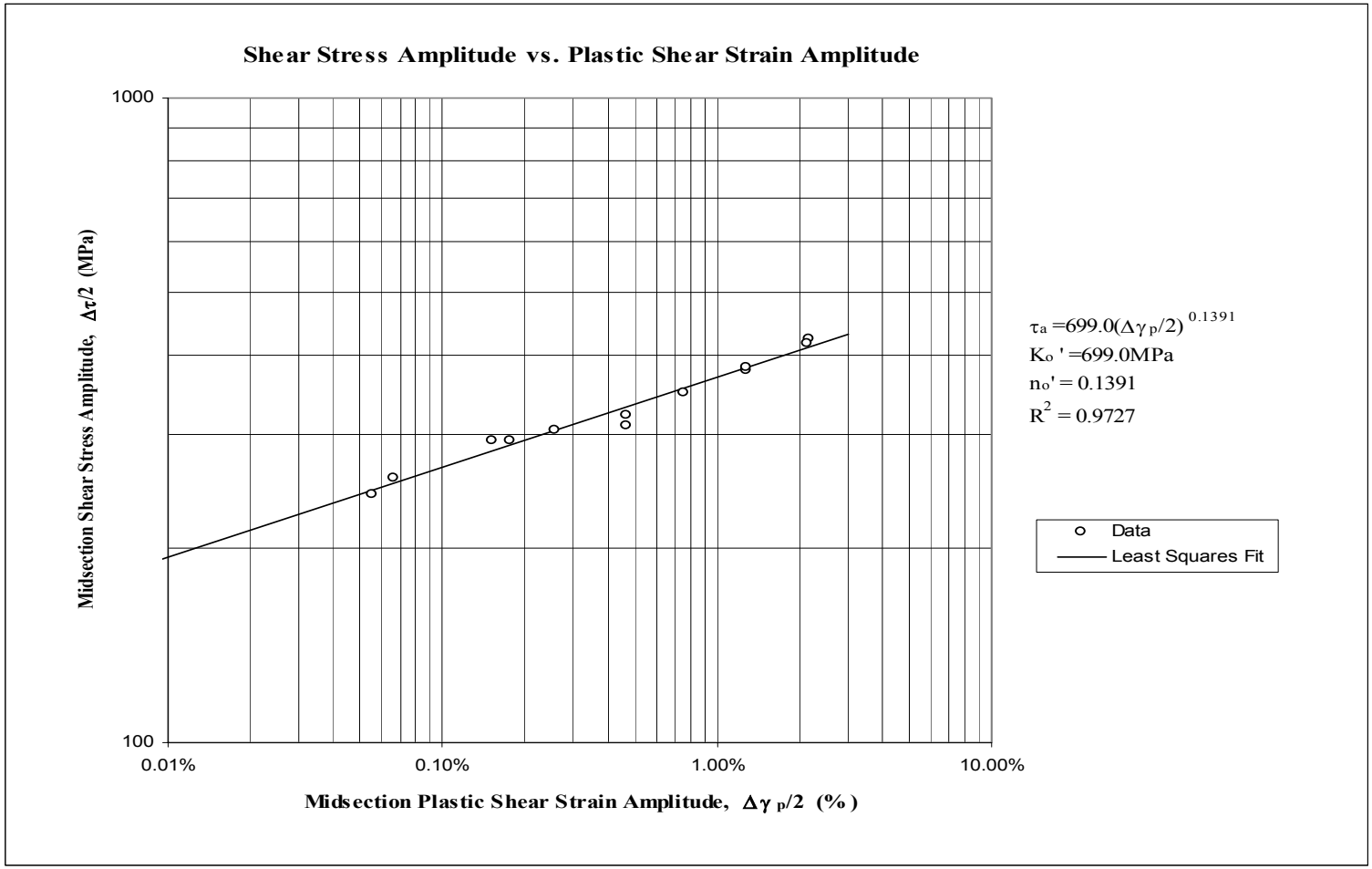

Figure 5: Shear stress amplitude versus plastic shear strain amplitude

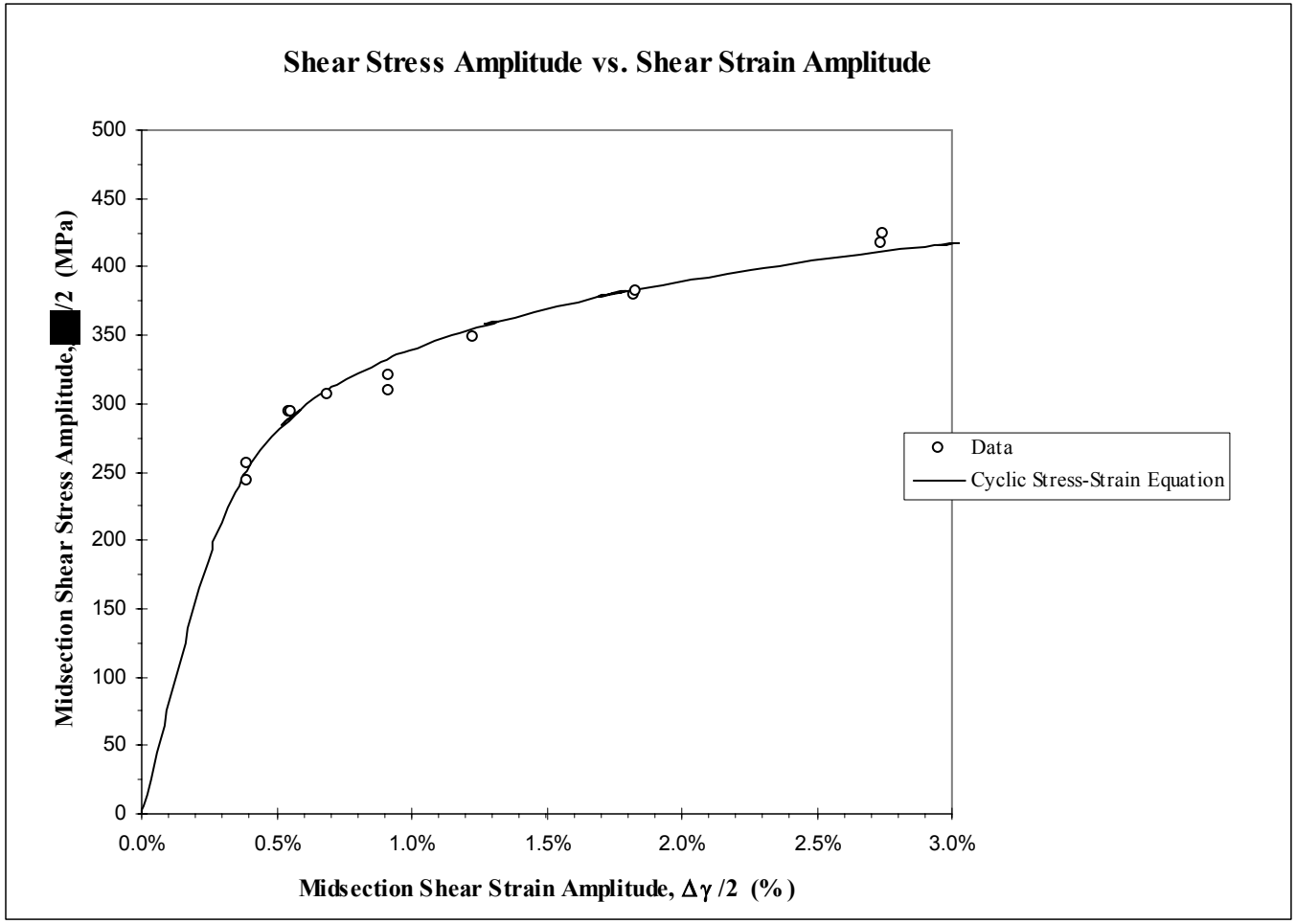

Figure 6: Shear stress amplitude versus shear strain amplitude

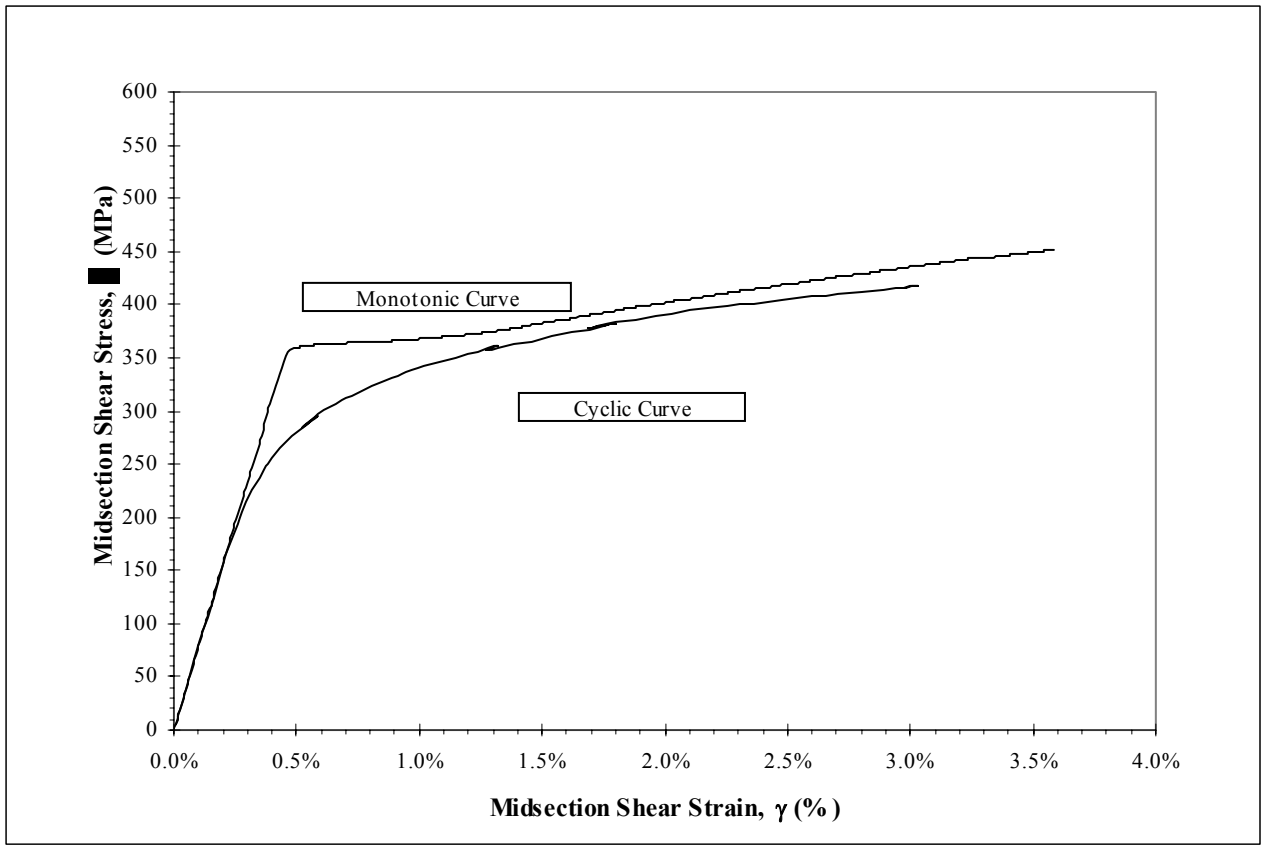

Figure 7: Composite plot of cyclic and monotonic shear stress-strain curves

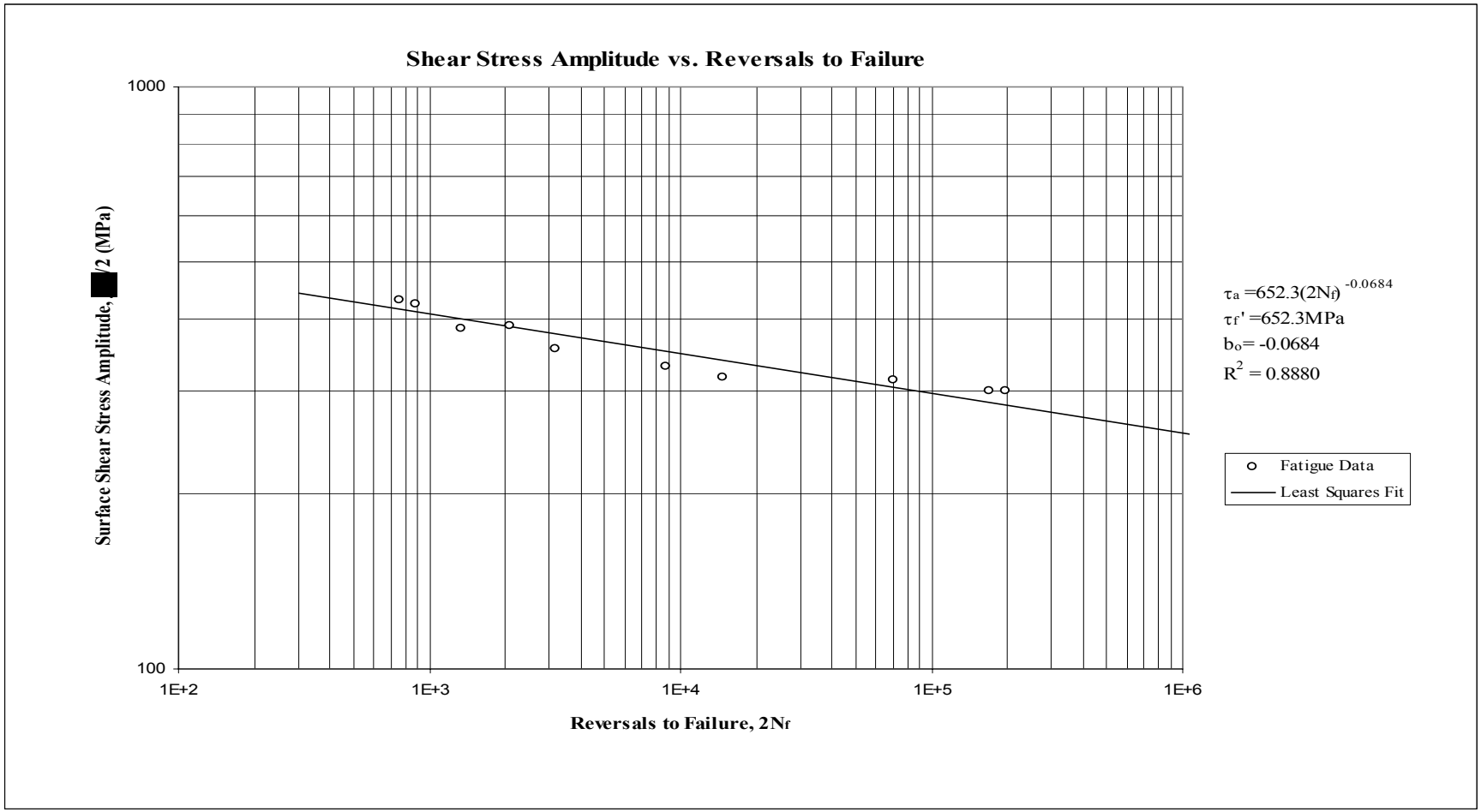

Figure 8: Shear stress amplitude versus reversals to failure

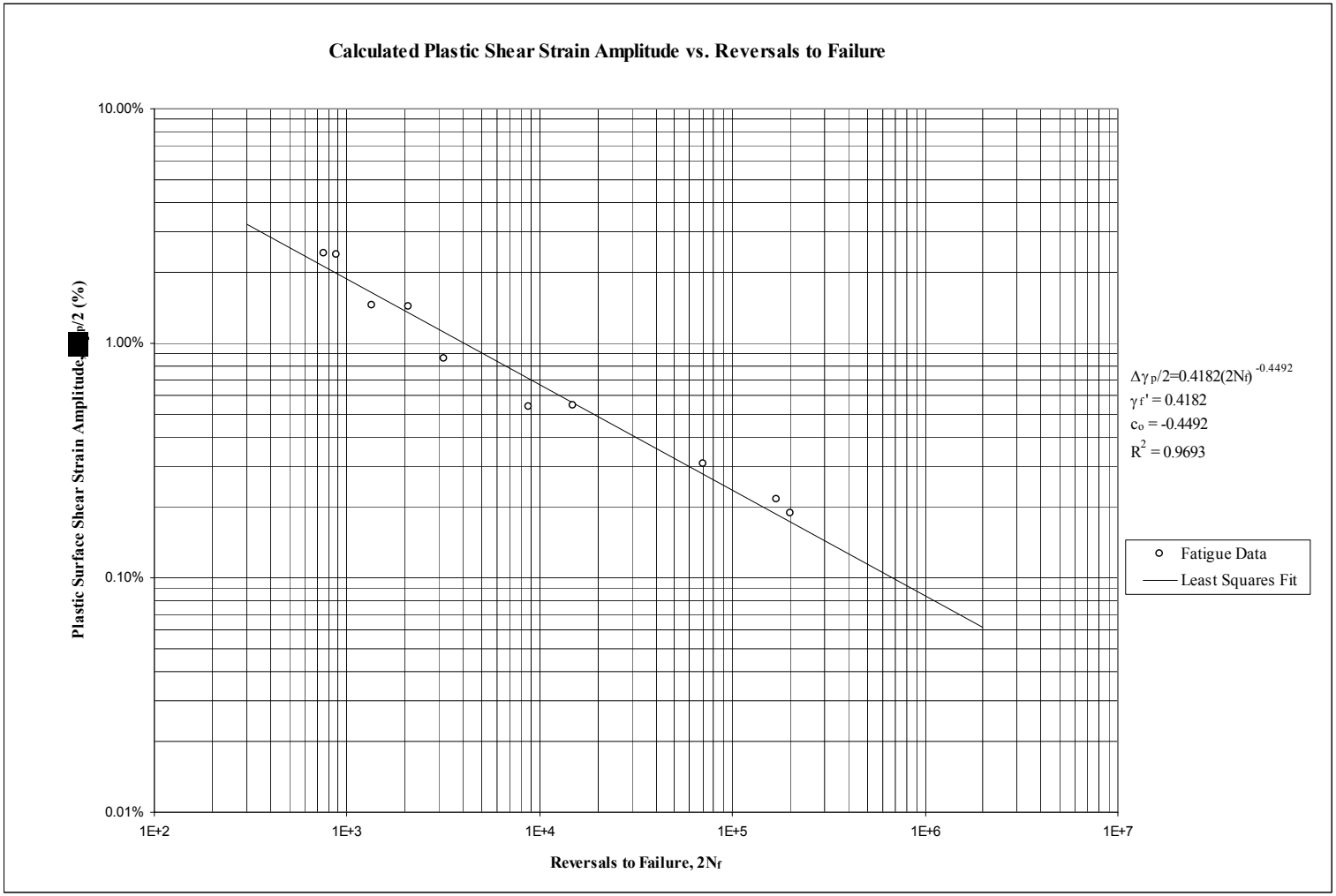

Figure 9: Calculated plastic shear strain amplitude versus reversals to failure

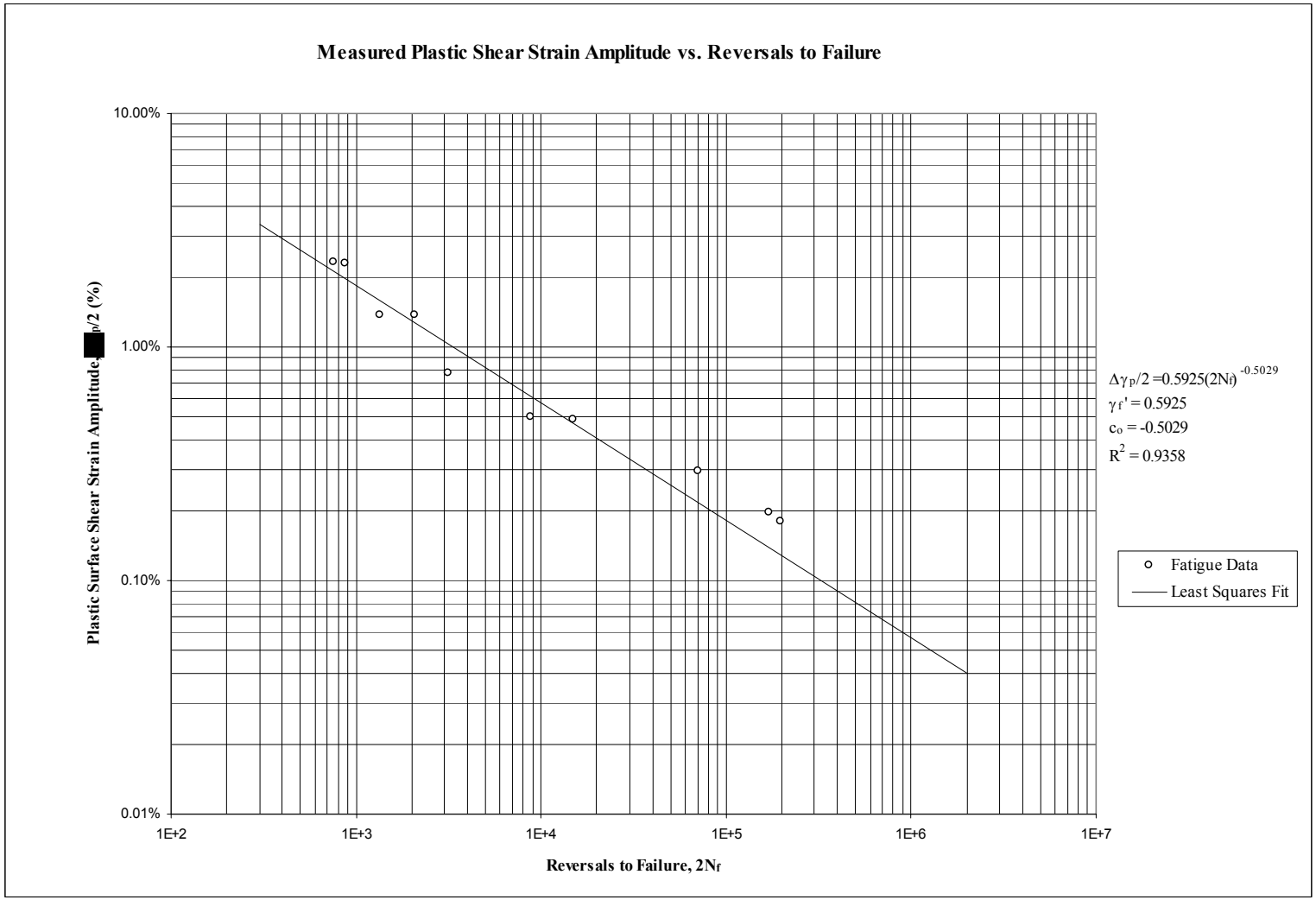

Figure 10: Measured plastic shear strain amplitude versus reversals to failure

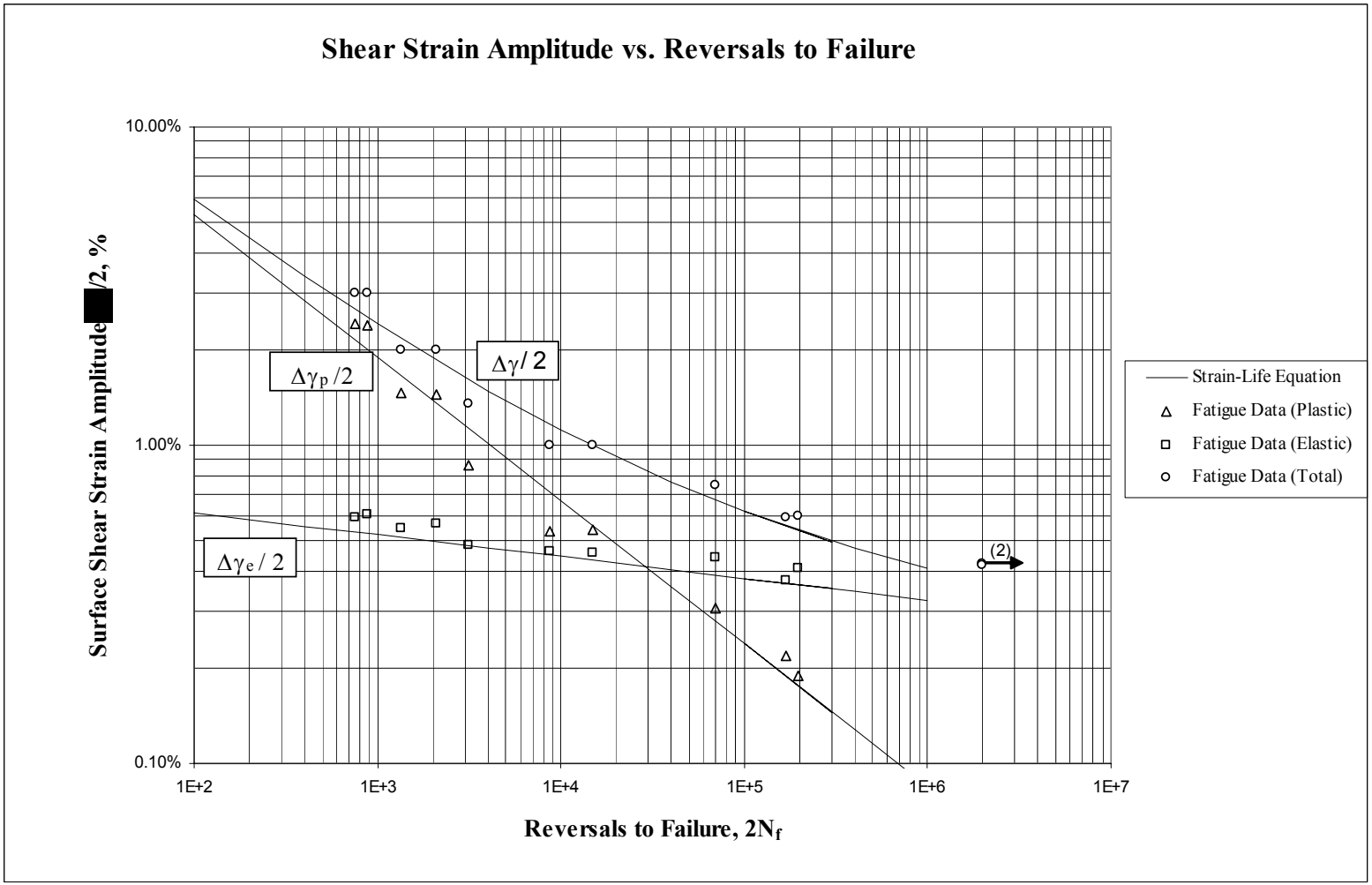

Figure 11: Shear strain amplitude versus reversals to failure

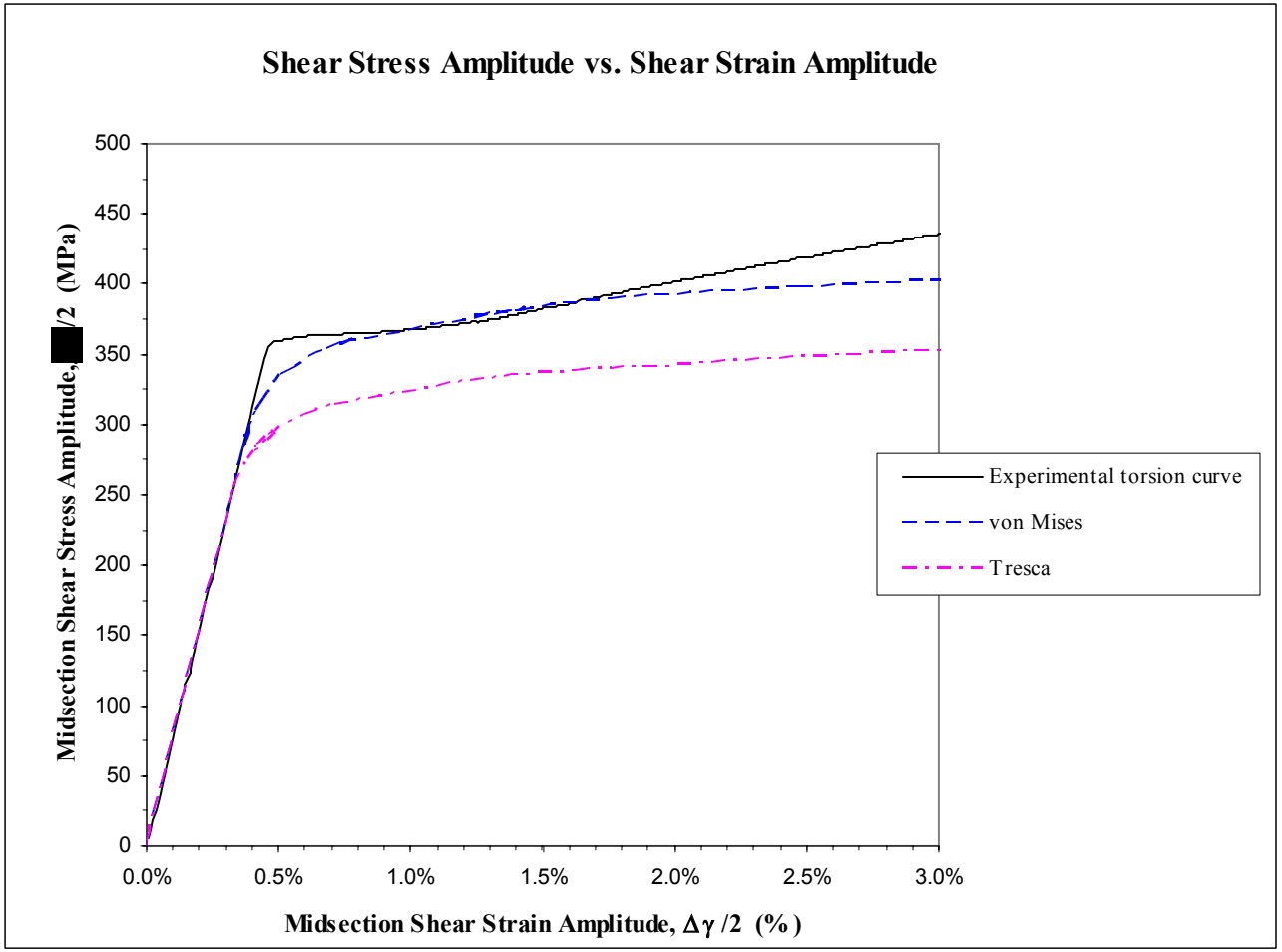

Figure 12: Comparison of monotonic torsion deformation curve with predictions based on von Mises and Tresca criteria using SAE 1045 steel (BHN 277) properties

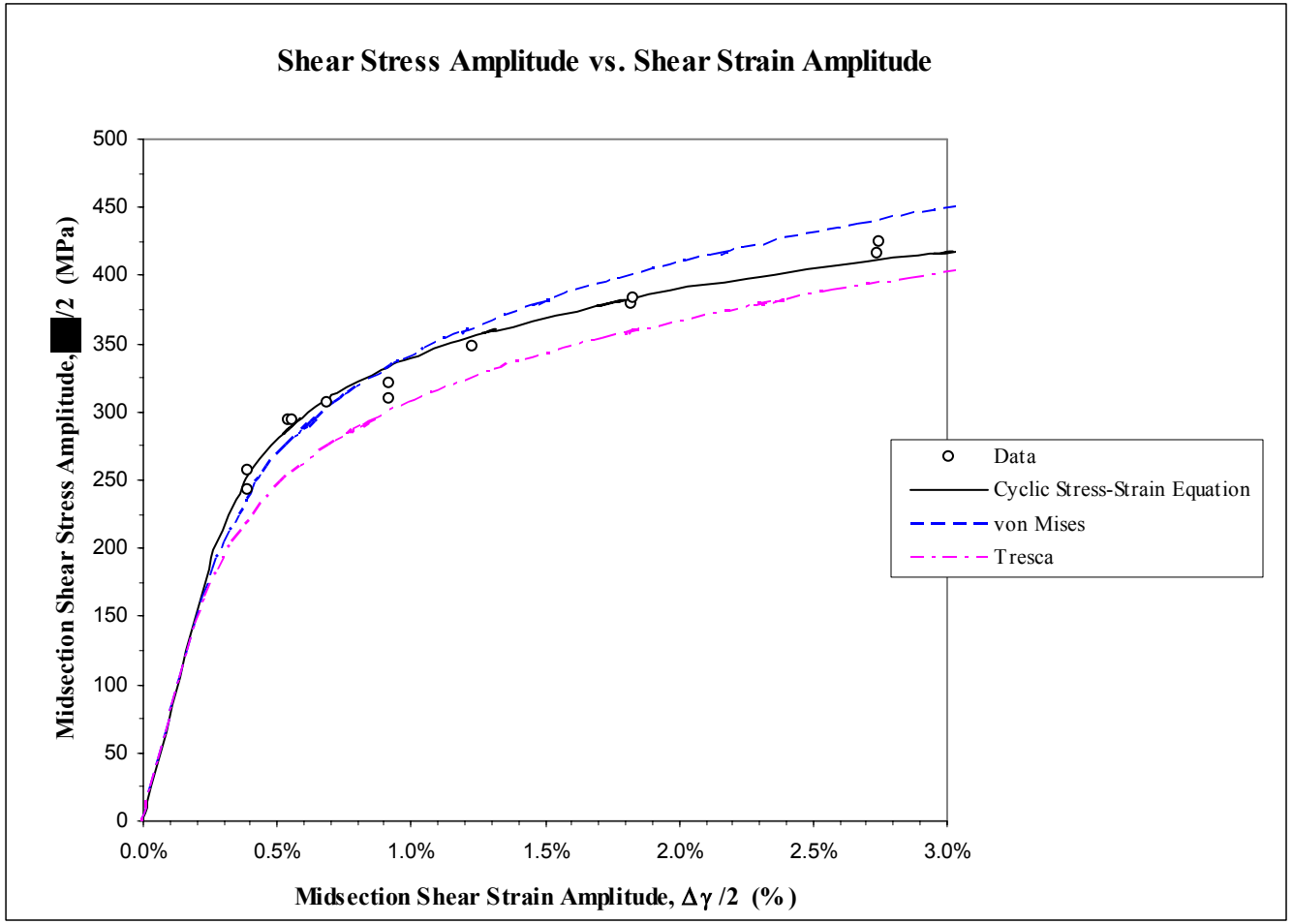

Figure 13: Torsional cyclic deformation curves based on test data and predictions using SAE 1045 steel (BHN 277) properties

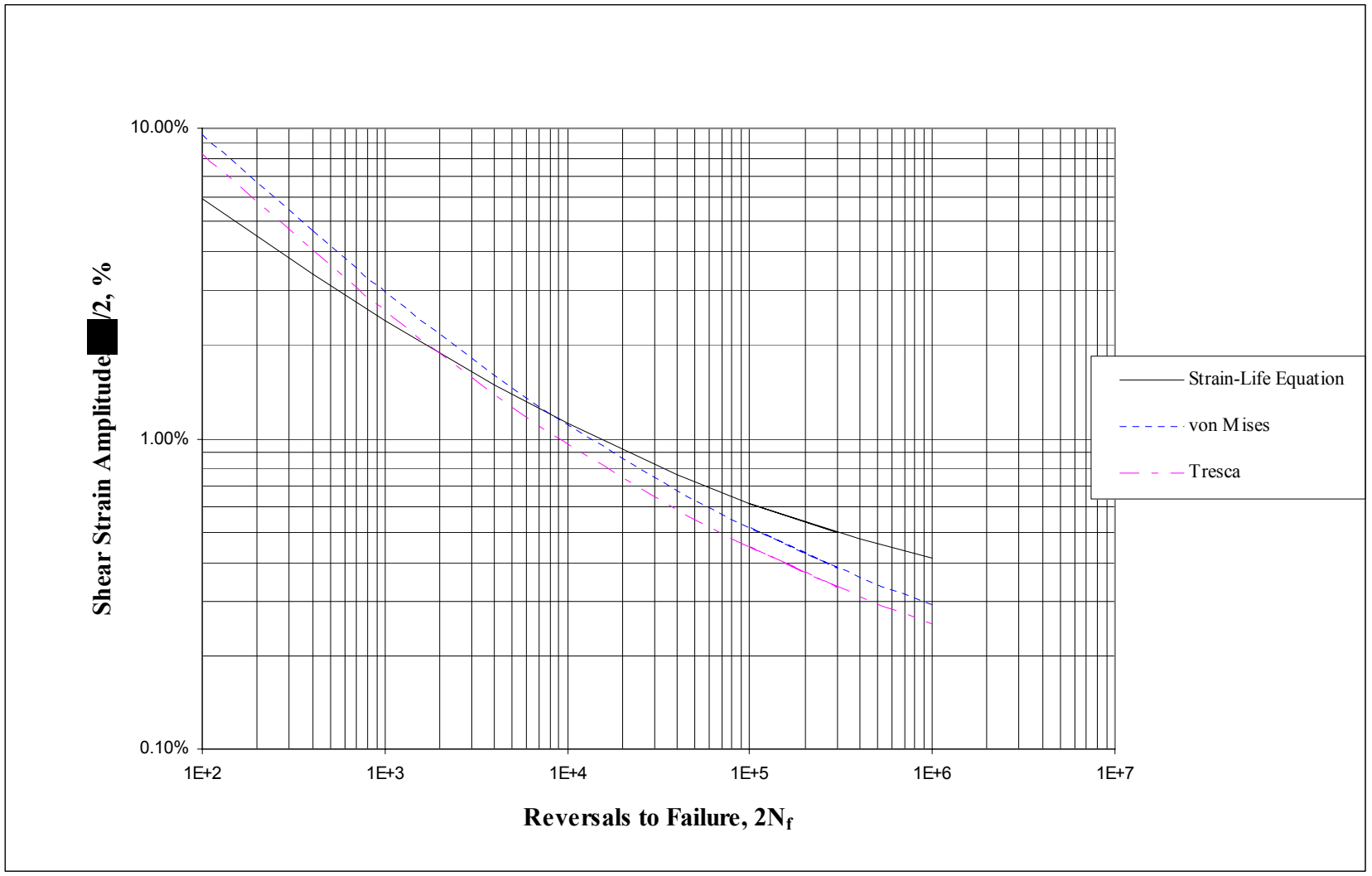

Figure 14: Total shear strain amplitude versus fatigue life from experiments and predictions based on SAE 1045 steel (BHN 277) properties

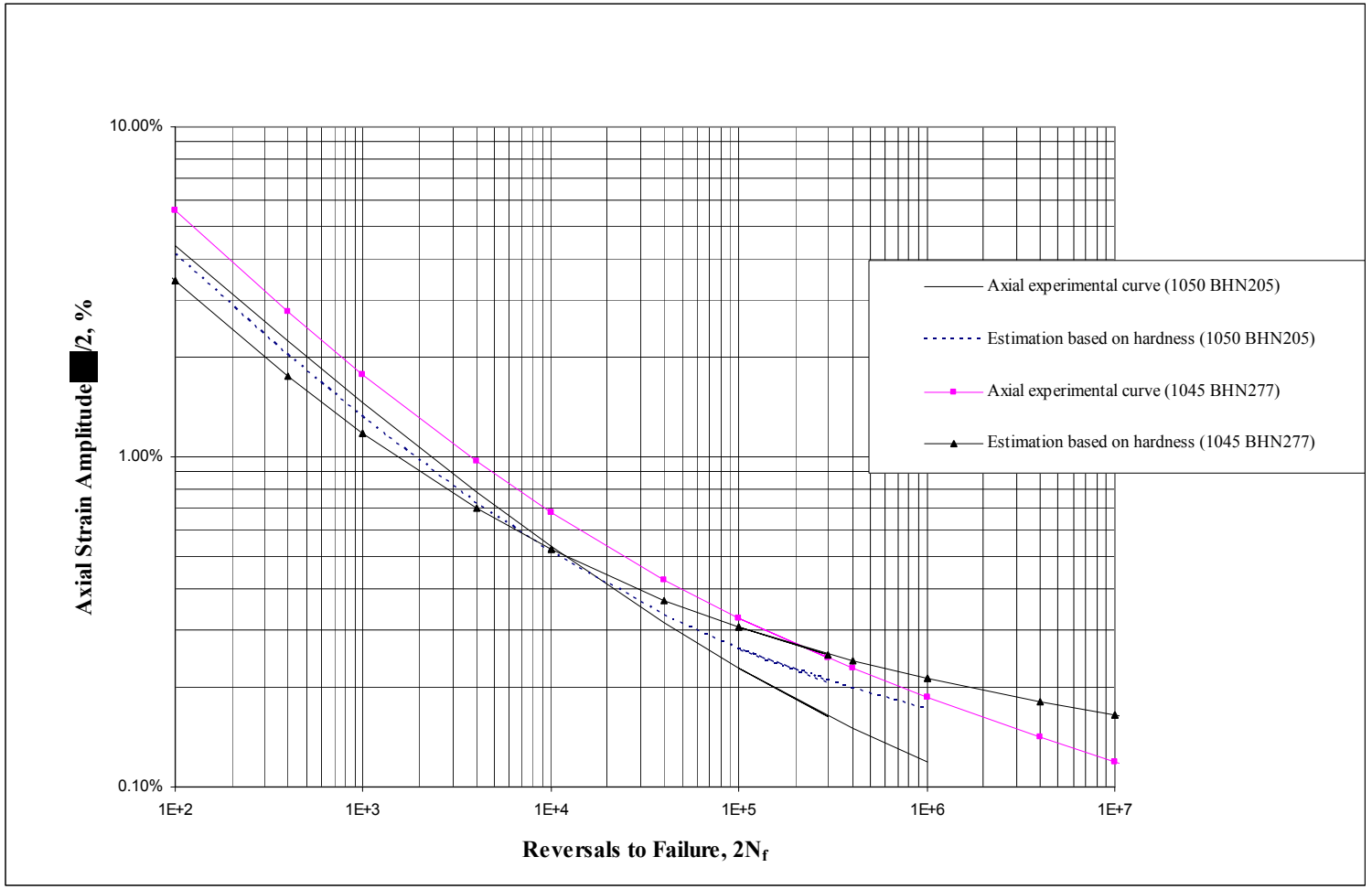

Figure 15: Comparison of experimental axial curve to axial strain-life prediction based on hardness using Roessle and Fatemi's method

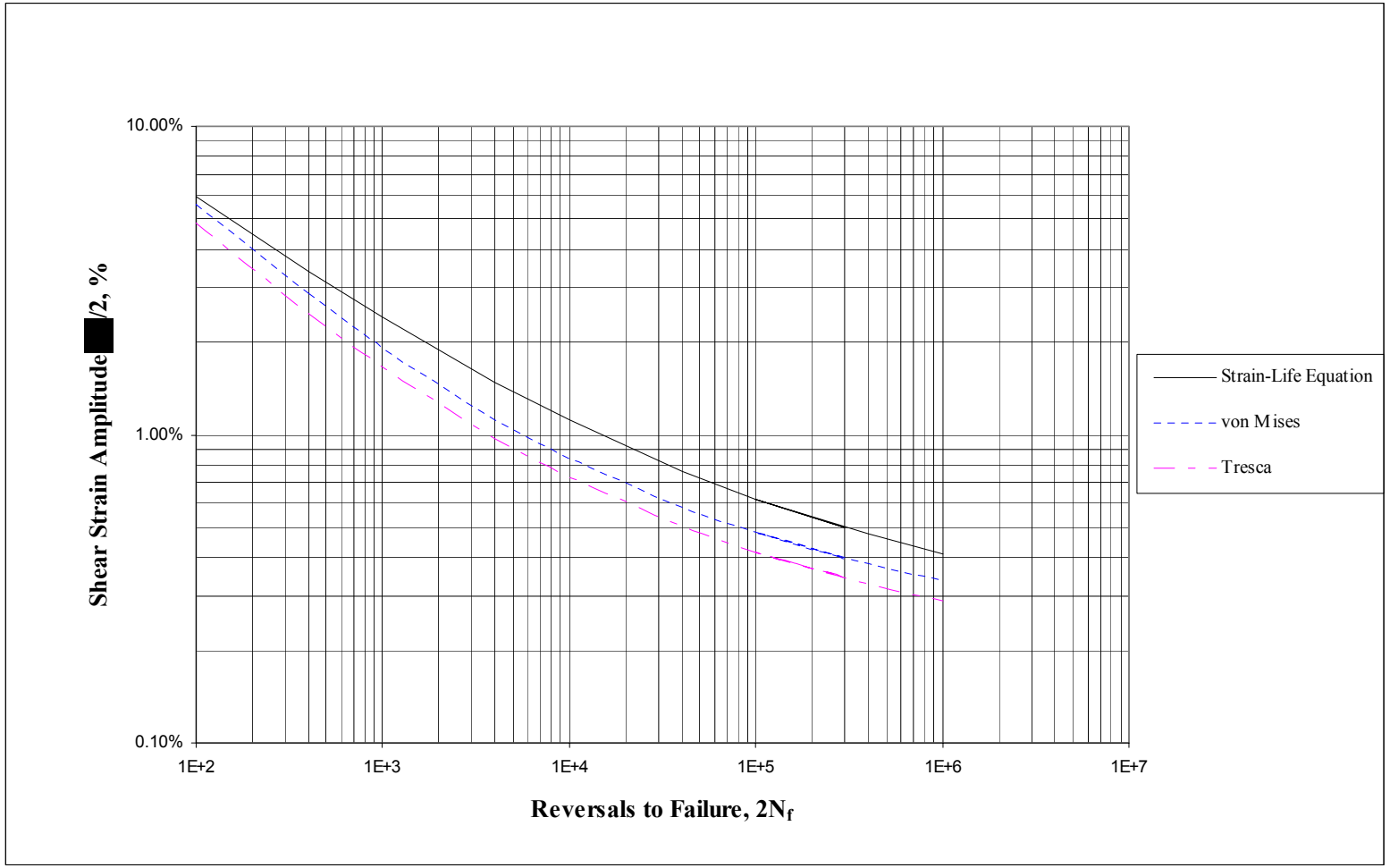

Figure 16: The total shear strain amplitude versus fatigue life from experiments and predictions based on hardness using Roessle and Fatemi's method

Figure 17: Specimen with longitudinal fatigue crack (specimen T 1, $N_f = 337$)

APPENDIX

Table A.1: Summary of Monotonic Properties for SAE 1050 Quenched and Tempered Steel

Specimen	OD, mm (in.)	ID, mm (in.)	G, GPa (ksi)	τ_y (0.2% offset), MPa (ksi)	τ_u, MPa (ksi)	K_0, MPa (ksi)	n_0	τ_f, MPa (ksi)	γ_f
T5	15.45 (0.6084)	12.70 (0.5001)	77.8 (11278)	366.5 (53.15)	585.7 (84.95)	780.81 (113.2)	0.1574	335.6 (48.68)	N/A

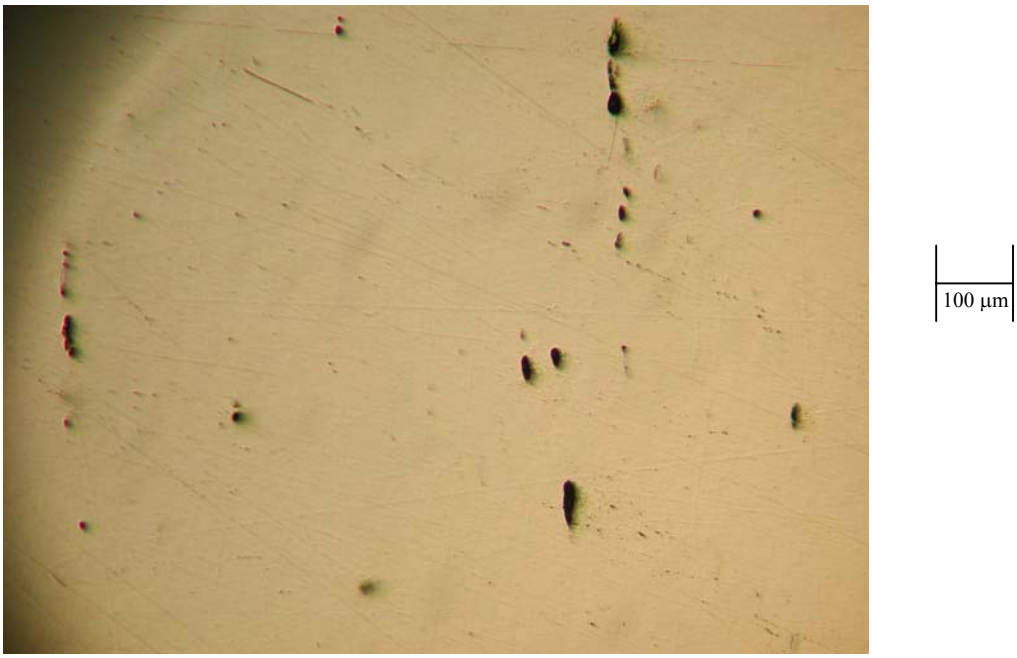

Figure A.1: Examples of inclusions in the longitudinal direction (L-T) at 100X for SAE 1050 quenched and tempered steel (rolling direction is horizontal)

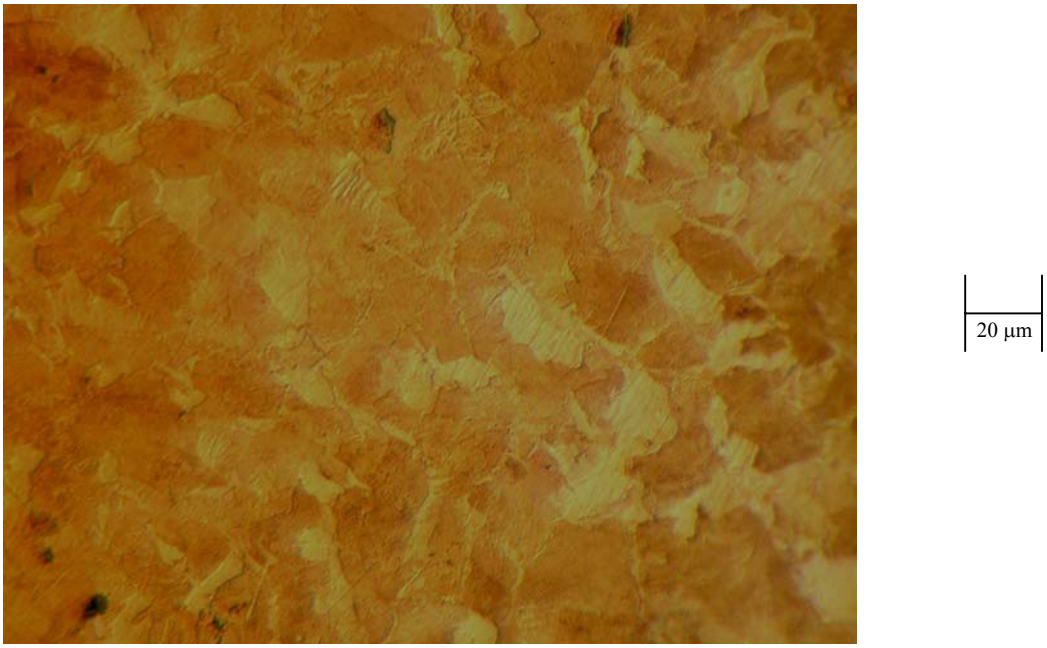

Figure A.2: Photomicrograph in the longitudinal direction (L-T) at 500X for SAE 1050 quenched and tempered steel (rolling direction is horizontal)

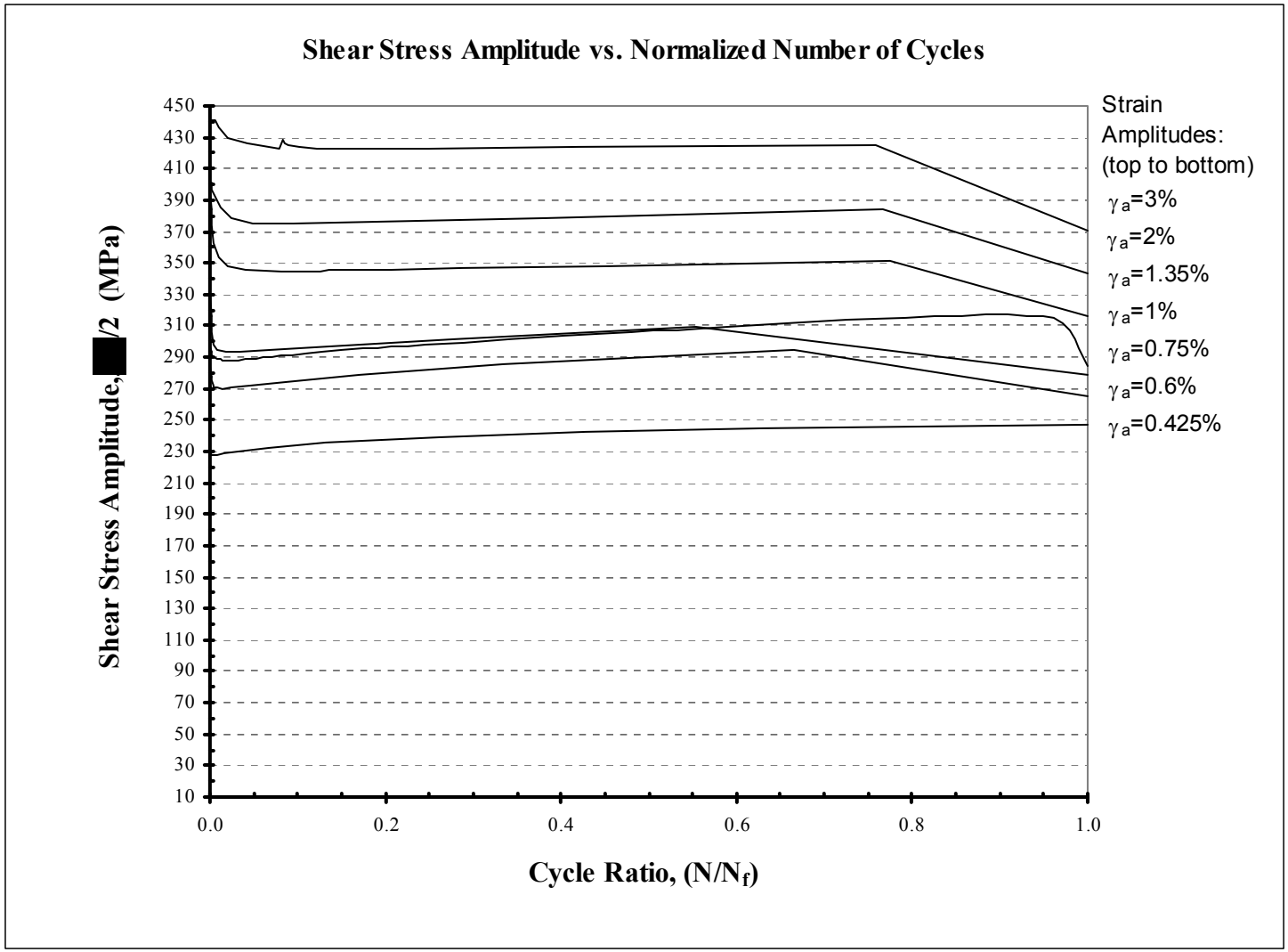

Figure A.2: Shear stress amplitude versus normalized number of cycles

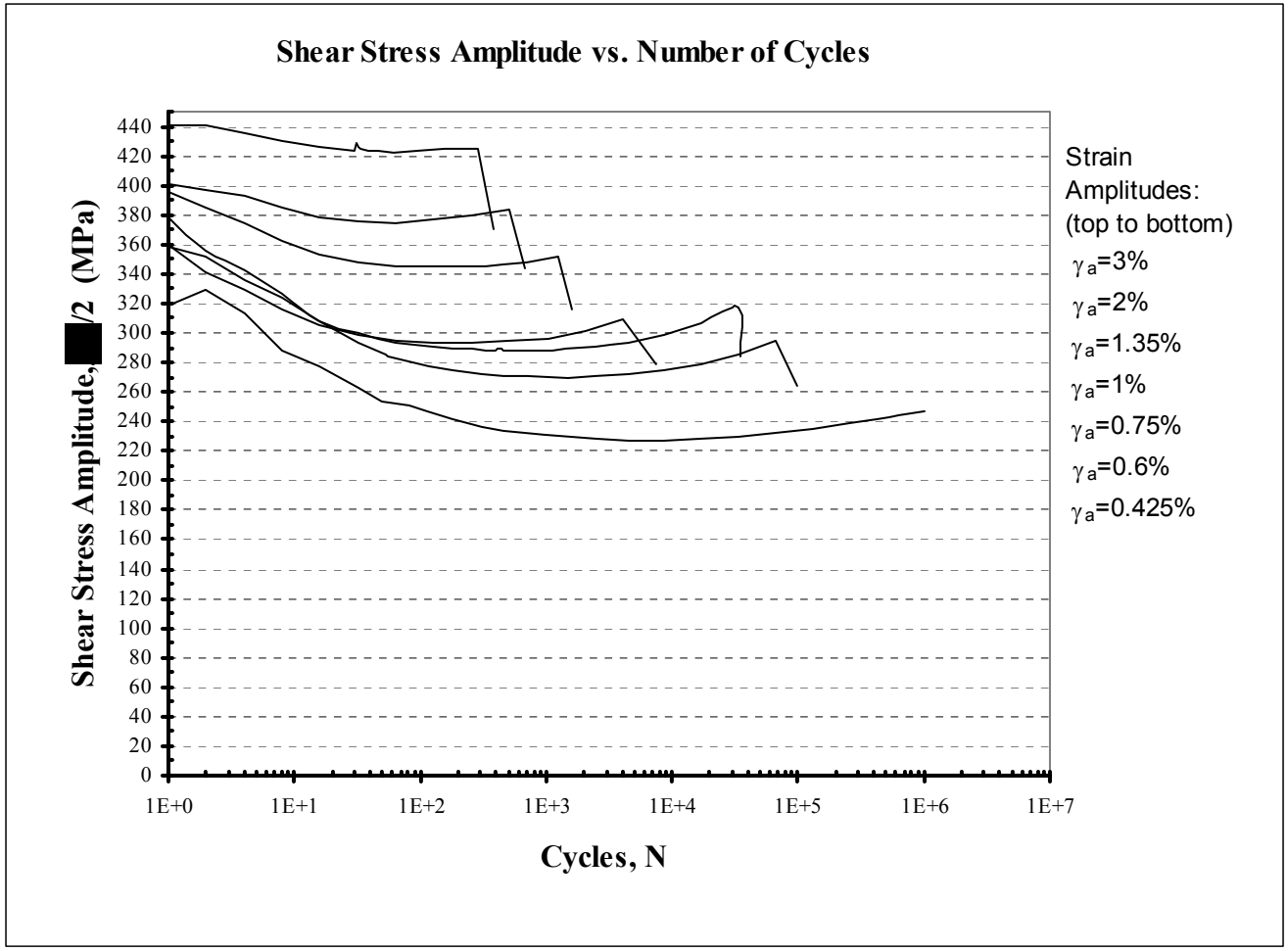

Figure A.3: Shear stress amplitude versus number of cycles

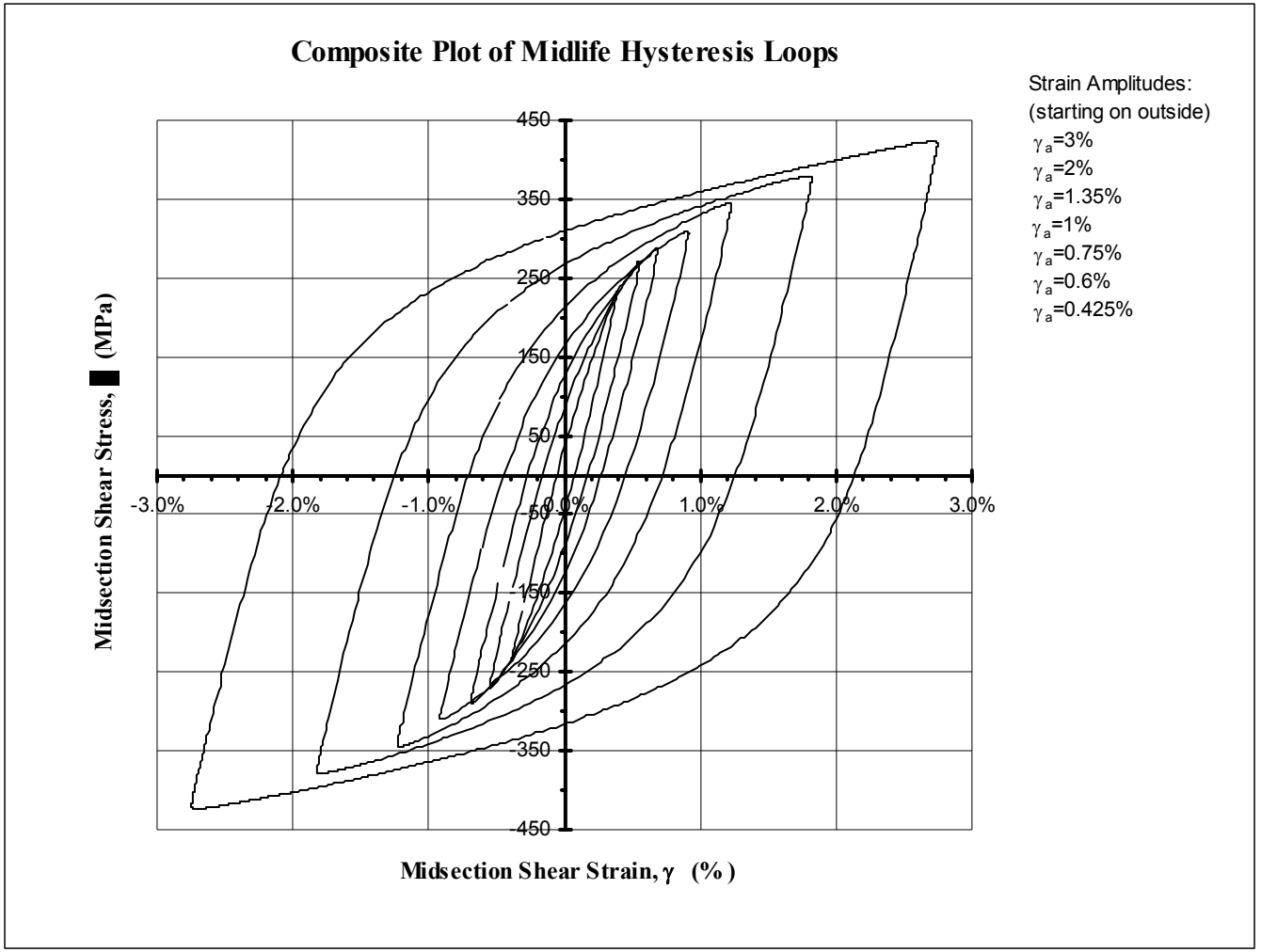

Figure A.4: Composite plot of midlife hysteresis loops